Future Global Meteorological Drought Hot Spots: A Study Based on CORDEX Data

JONATHAN SPINONI,[a] PAULO BARBOSA,[a] EDOARDO BUCCHIGNANI,[b] JOHN CASSANO,[c] TEREZA CAVAZOS,[d] JENS H. CHRISTENSEN,[e,f,bb] OLE B. CHRISTENSEN,[f] ERIKA COPPOLA,[g] JASON EVANS,[h] BEATE GEYER,[i] FILIPPO GIORGI,[g] PANOS HADJINICOLAOU,[j] DANIELA JACOB,[k] JACK KATZFEY,[l] TORBEN KOENIGK,[m] RENÉ LAPRISE,[n] CHRISTOPHER J. LENNARD,[o] M. LEVENT KURNAZ,[p,q] DELEI LI,[r] MARTA LLOPART,[s] NIALL MCCORMICK,[a] GUSTAVO NAUMANN,[a] GRIGORY NIKULIN,[m] TUGBA OZTURK,[t] HANS-JUERGEN PANITZ,[u] ROSMERI PORFIRIO DA ROCHA,[v] BURKHARDT ROCKEL,[i] SILVINA A. SOLMAN,[w,x] JOZEF SYKTUS,[y] FREDOLIN TANGANG,[z] CLAAS TEICHMANN,[k] ROBERT VAUTARD,[aa], JÜRGEN V. VOGT,[a] KATJA WINGER,[n] GEORGE ZITTIS,[j] AND ALESSANDRO DOSIO[a]

[a] *European Commission, Joint Research Centre, Ispra, Italy*
[b] *Centro Euro-Mediterraneo sui Cambiamenti Climatici, Lecce, Italy*
[c] *Cooperative Institute for Research in Environmental Sciences, and Department of Atmospheric and Oceanic Sciences, University of Colorado Boulder, Boulder, Colorado*
[d] *Centro de Investigacion Cientifica y de Educacion Superior de Ensenada, Ensenada, Mexico*
[e] *Niels Bohr Institute, University of Copenhagen, Copenhagen, Denmark*
[f] *Danish Meteorological Institute, Copenhagen, Denmark*
[g] *Abdus Salam International Centre for Theoretical Physics, Trieste, Italy*
[h] *Faculty of Science, University of New South Wales, Sydney, New South Wales, Australia*
[i] *Helmholtz-Zentrum Geesthacht, Institute of Coastal Research, Hamburg, Germany*
[j] *Energy, Environment and Water Research Center, Cyprus Institute, Nicosia, Cyprus*
[k] *Climate Service Center Germany, Hamburg, Germany*
[l] *Commonwealth Scientific and Industrial Research Organisation Marine and Atmospheric Research, Aspendale, Victoria, Australia*
[m] *Rossby Centre, Swedish Meteorological and Hydrological Institute, Norrkoping, Sweden*
[n] *Département des Sciences de la Terre et de l'Atmosphère, University du Quebec à Montreal, Montreal, Quebec, Canada*
[o] *Climate System Analysis Group, University of Cape Town, Cape Town, South Africa*
[p] *Department of Physics, Faculty of Arts and Sciences, Bogazici University, Istanbul, Turkey*
[q] *Center for Climate Change and Policy Studies, Bogazici University, Istanbul, Turkey*
[r] *Chinese Academy of Sciences, Institute of Oceanology, Qingdao, China*
[s] *Sao Paulo State University and Bauru Meteorological Centre (IPMet/UNESP), Bauru, Sao Paulo, Brazil*
[t] *Department of Physics, Faculty of Arts and Sciences, Isik University, Istanbul, Turkey*
[u] *Institute of Meteorology and Climate Research, Karlsruhe Institute of Technology, Karlsruhe, Germany*
[v] *Departimento de Ciências Atmosféricas, Universidade de Sao Paulo, Sao Paulo, Brazil*
[w] *Facultad de Ciencias Exactas y Naturales, Departamento de Ciencias de la Atmósfera y los Océanos, Universidad de Buenos Aires, Buenos Aires, Argentina*
[x] *Centro de Investigaciones del Mar y la Atmósfera, Universidad de Buenos Aires, Buenos Aires, Argentina*
[y] *Global Change Institute, University of Queensland, Brisbane, Queensland, Australia*
[z] *Department of Earth Sciences and Environment, The National University of Malaysia (UKM), Selangor, Malaysia*
[aa] *National Centre for Scientific Research, Laboratoire des Sciences du Climat et de l'Environment, Gif-sur-Yvette, France*
[bb] *Norwegian Research Centre AS (NORCE), Bergen, Norway*

(Manuscript received 30 January 2019, in final form 28 November 2019)

Denotes content that is immediately available upon publication as open access.

Corresponding author: Jonathan Spinoni, jonathan.spinoni@ec.europa.eu

DOI: 10.1175/JCLI-D-19-0084.1

ABSTRACT

Two questions motivated this study: 1) Will meteorological droughts become more frequent and severe during the twenty-first century? 2) Given the projected global temperature rise, to what extent does the inclusion of temperature (in addition to precipitation) in drought indicators play a role in future meteorological droughts? To answer, we analyzed the changes in drought frequency, severity, and historically undocumented extreme droughts over 1981–2100, using the standardized precipitation index (SPI; including precipitation only) and standardized precipitation-evapotranspiration index (SPEI; indirectly including temperature), and under two representative concentration pathways (RCP4.5 and RCP8.5). As input data, we employed 103 high-resolution (0.44°) simulations from the Coordinated Regional Climate Downscaling Experiment (CORDEX), based on a combination of 16 global circulation models (GCMs) and 20 regional circulation models (RCMs). This is the first study on global drought projections including RCMs based on such a large ensemble of RCMs. Based on precipitation only, ~15% of the global land is likely to experience more frequent and severe droughts during 2071–2100 versus 1981–2010 for both scenarios. This increase is larger (~47% under RCP4.5, ~49% under RCP8.5) when precipitation and temperature are used. Both SPI and SPEI project more frequent and severe droughts, especially under RCP8.5, over southern South America, the Mediterranean region, southern Africa, southeastern China, Japan, and southern Australia. A decrease in drought is projected for high latitudes in Northern Hemisphere and Southeast Asia. If temperature is included, drought characteristics are projected to increase over North America, Amazonia, central Europe and Asia, the Horn of Africa, India, and central Australia; if only precipitation is considered, they are found to decrease over those areas.

1. Introduction

The latter decades of the twentieth century and the early years of the twenty-first century have seen many extreme weather events, among which heat waves and extreme precipitation in particular have become increasingly frequent in many global areas (IPCC 2014). Compared to other natural disasters such as floods or storms, detecting and quantifying droughts is more complex, since droughts are characterized by a slow onset and a high resilience to their effects, while long-term impacts may emerge months or even years after the drought peak (Vogt and Somma 2000; Wilhite 2000; Wilhite et al. 2007). Another level of complexity arises from the many different definitions of drought, including meteorological, agricultural, hydrological, socioeconomic, and ecological droughts (Mishra and Singh 2010; Crausbay et al. 2017). Different types of droughts can lead to different, often cascading impacts, affecting various economic sectors such as agriculture (Schmidhuber and Tubiello 2007; Li et al. 2009), hydroelectric and thermal power generation (Bartos and Chester 2015), public water supply (Iglesias et al. 2009), waterborne transport, and tourism (Thomas et al. 2013). Environmental and social impacts include, for example, vegetation stress (Vicente-Serrano et al. 2013), wetland, soil and land degradation (Bai et al. 2008), and links with migration (Kelley et al. 2015). Consequently, the recognition of drought as a climate hazard, as well as a better understanding of its manifold aspects, is becoming an urgent priority in a warming world (Dai 2011), with the result that drought is becoming a "hot topic" in climatology (Trenberth et al. 2014).

In this study, we focus on meteorological drought, which is caused by a prolonged rainfall deficit, often enhanced by other meteorological conditions, such as high temperatures, high evapotranspiration rates, and desiccating winds (Palmer 1965; Wilhite and Glantz 1985). In recent decades, many studies have reported an overall global tendency toward more frequent and severe meteorological drought events (e.g., Dai 2011, 2013; Spinoni et al. 2014; Osborn et al. 2016), even though the consensus about the extent and magnitude of the change is not universal (Seneviratne 2012; Sheffield et al. 2012; Hauser et al. 2017). Although most studies agree on the location of recent past drought hot spots—namely, the Mediterranean region, western North America, southern South America, large parts of Africa, and northeastern China (Trenberth et al. 2014; Spinoni et al. 2015a; Coelho et al. 2016; Cook et al. 2016; Dai and Zhao 2017; Zittis 2018)—other regions have also been hit by megadroughts in recent years. Examples are western North America including Mexico from 1999 to 2007 (Stahle et al. 2009), Australia from 2001 to 2009 (van Dijk et al. 2013), Russia in 2010 (Wegren 2011), California in 2013–14 (S. Wang et al. 2014), Europe over the last two decades (Hanel et al. 2018), South Africa in 2015–18 (Masante et al. 2018), and Kenya in 2014–19 (Reliefweb 2019).

In contrast with past events, the overall picture for meteorological drought projections is still incomplete. A number of studies investigated multimodel hydrological and meteorological drought projections based on global climate models (GCMs) of previous (e.g., CMIP3; Seager et al. 2007; Sheffield and Wood 2008; Dai 2011;

Orlowsky and Seneviratne 2012) and current generations (CMIP5; Prudhomme et al. 2014; Touma et al. 2015; Ukkola et al. 2018). However, such projections are often presented with medium spatial resolution (i.e., not better than 1°) and sometimes using only a limited number of simulations. Due to such limitations, most projections suffer from large uncertainties (Burke and Brown 2008; Dai 2013; Orlowsky and Seneviratne 2013; Zhao and Dai 2017; Lu et al. 2019). On the other hand, some studies investigated drought hazard projections on selected countries or regions (Cook et al. 2015; Spinoni et al. 2018) by means of regional climate models (RCMs).

This study aims at improving the available meteorological drought projections by using—for the first time, to our knowledge—a large number of simulations (103) based on a combination of GCMs and RCMs, and producing high spatial resolution (0.44° or ~50 km) global projections of drought frequency, severity, and peak events (i.e., historically undocumented extreme droughts) for the twenty-first century. The RCMs are guided by the parent GCMs but, being able to represent small-scale processes and features (Rummukainen 2010), they have been shown to simulate more accurately present-day, observed precipitation characteristics and higher-order statistics, and in turn to "add value" to the performances of GCMs (Feser et al. 2011; Di Luca et al. 2012; Giorgi et al. 2014; Dosio et al. 2015; Torma et al. 2015; Kendon et al. 2017; Dosio et al. 2019). Consequently, as we discuss in section 3, the use of RCMs, coupled with GCMs, can help showing drought-related spatial patterns that the use of GCMs alone cannot provide.

We considered two climate scenarios: the moderate representative concentration pathway (RCP) 4.5 and the more extreme RCP8.5 (van Vuuren et al. 2011). The RCM simulations were produced in the framework of the Coordinated Regional Climate Downscaling Experiment (CORDEX; www.cordex.org) at a spatial resolution of 0.44°. Although some CORDEX simulations have previously been used in drought-related studies at regional scale (e.g., Meresa et al. 2016; Zahradníček et al. 2016; Diasso and Abiodun 2017; Um et al. 2017; Spinoni et al. 2018; Tabari and Willems 2018), they have never been applied for global-scale drought analyses.

This study also aims to answer the following question: where and to what extent will the projected temperature rise (IPCC 2014) play a crucial role in increased drought frequency and severity? Similar to a previous study focused on Europe (Spinoni et al. 2018), here we separately investigated drought projections based on both standardized precipitation index (SPI; McKee et al. 1993) and standardized precipitation-evapotranspiration index (SPEI; Vicente-Serrano et al. 2010), in order to evaluate the importance of including temperature in drought projections. SPI uses only precipitation as input (Spinoni et al. 2014), while SPEI uses both precipitation and potential evapotranspiration, which incorporates the effects of temperature (Beguería et al. 2014).

This is not the first attempt to investigate global drought projections using different drought indicators: Touma et al. (2015) compared four indicators, including the SPI and the SPEI, using the results of 15 GCMs. They regridded the outputs at common 1° resolution, unavoidably introducing an interpolation bias because only 2 of the 15 GCMs used have a spatial resolution comparable to 1°. In our study, the use of RCMs—over the native common 0.44° grid—allows a higher resolution without the need to regrid the outputs. Moreover, the larger number of simulations, especially over some regions, allows deeper evaluation of the uncertainties and more robust analysis of statistical significance of projected changes.

The remainder of this paper is structured in three main sections. In section 2, the data and methods are described, with a focus on the CORDEX dataset, the drought indicators, and the definition of drought-related variables. In section 3, the increase or decrease in drought frequency and severity from 1981–2010 to 2071–2100, both at global and macroregional spatial scale, are analyzed. The relative importance of temperature and/or precipitation as meteorological drivers for future droughts, is also discussed in section 3, focusing on areas where the two drought indicators result in diverging projections. Section 4 summarizes the results of the study and anticipates possible further steps.

2. Data and methods

a. *Input data: Gathering macroregional CORDEX simulations*

The CORDEX initiative is a World Climate Research Programme (WCRP) core project (Giorgi et al. 2009; Giorgi and Gutowski 2015), which has promoted the provision of climate information at regional scale by means of coordinated regional climate downscaling (RCD) techniques (Hewitson and Crane 1996), over several continental regions of the world. Different institutions and research groups (for the complete list, see www.cordex.org) have contributed to producing climate outputs based on a variety of RCMs over 14 geographical domains, covering the main continental areas of the world (see Table 1).

The CORDEX outputs consist of multivariable time series at different spatial and time resolutions and climate scenarios. For each CORDEX domain (i.e., region), a set of simulations is available, depending on the combinations of GCMs and RCMs. For our purposes, only the simulations including data for daily

TABLE 1. CORDEX domains and combinations of GCMs and RCMs available for each region. The letter C before the acronym is introduced to avoid confusion with the macroregions shown in Fig. 2 and used for regional statistics. CSIRO-CCAM is a global model with a stretched grid.

CORDEX region	RCM	GCM
C-AFR (Africa)	CCCma-CanRCM4	CanESM2
	CLMcom-CCLM4–8-17	CNRM-CM5; HadGEM2-ES; ICHEC-EC-EARTH; MPI-ESM-LR
	DMI-HIRHAM5	ICHEC-EC-EARTH; NorESM1-M
	KNMI-RACMO22T	HadGEM2-ES; ICHEC-EC-EARTH
	MPI-CSC-REMO2009	ICHEC-EC-EARTH; MPI-ESM-LR
	SMHI-RCA4	CanESM2; CNRM-CM5; CSIRO-MK3–6-0; GFDL-ESM2M; HadGEM2-ES; ICHEC-EC-EARTH; IPSL-CM5A-MR; MIROC5; Nor-ESM1-M
C-ANT (Antarctica)	DMI-HIRHAM5	ICHEC-EC-EARTH
	KNMI-RACMO21P	HadGEM2-ES; ICHEC-EC-EARTH
C-ARC (Arctic)	CCCma-CanRCM4	CanESM2
	DMI-HIRHAM5	ICHEC-EC-EARTH
	SMHI-RCA4	CanESM2; ICHEC-EARTH; MPI-ESM-LR; NorESM1-M
	SMHI-RCA4-GUESS	ICHEC-EC-EARTH
C-AUS (Australia)	CSIRO-CCAM	ACCESS-1.0; CCSM4; GFDL-CM3; CNRM-CM5; MPI-ESM-LR; NorESM1-M
	CLMcom-CCLM4.8-17-CLM3.5	ICHEC-EC-EARTH; MPI-ESM-LR
C-CAM (Central America)	SMHI-RCA4	HadGEM2-ES; ICHEC-EC-EARTH; MPI-ESM-LR
C-CAS (Central Asia)	BOUN-RegCM4.3	HadGEM2-ES; MPI-ESM-MR
C-EAS (East Asia)	CLMcom-CCLM5–0-2	CNRM-CM5; HadGEM2-ES; ICHEC-EC-EARTH; MPI-ESM-LR
	DMI-HIRHAM5	ICHEC-EC-EARTH
	MOHC-HadGEM3-RA	ICHEC-EC-EARTH
C-EUR (Europe)	CCCma-CanRCM4	CanESM2
	CLMcom-CCLM4.8-17	MPI-ESM-LR
	CNRM-ALADIN53	CNRM-CM5
	DMI-HIRHAM5	ICHEC-EC-EARTH
	IPSL-INERIS-WRF331F	IPSL-CM5A-MR
	KNMI-RACMO22E	HadGEM2-ES; ICHEC-EC-EARTH
	MPI-CSC-REMO2009	MPI-ESM-LR
	SMHI-RCA4	CanESM2; CNRM-CM5; CSIRO-Mk3.6.0; GFDL-ESM2M; HadGEM2-ES; ICHEC-EC-EARTH; IPSL-CM5A-MR; MIROC5; MPI-ESM-LR; NorESM1-M
C-MED (Mediterranean)	CLMcom-CCLM4.8-18	MPI-ESM-LR
	CLMcom-CCLM4.8-19	CMCC-CM
	CNRM-ALADIN52	CNRM-CM5
	ICTP-RegCM4.3	HadGEM2-ES
C-MENA (Middle East, North Africa)	SMHI-RCA4	CNRM-CM5; GFDL-ESM2M; ICHEC-EC-EARTH;
	CYI-WRF351F	CESM1
C-NAM (North America)	CCCma-CanRCM4	CanESM2
	DMI-HIRHAM5	ICHEC-EC-EARTH
	SMHI-RCA4	CanESM2; ICHEC-EC-EARTH
	UQAM-CRCM5	CanESM2
C-SAM (South America)	ICTP-RegCM4.3	HadGEM2-ES
	MPI-CSC-REMO2009	MPI-ESM-LR
	SMHI-RCA4	CanESM2; CSIRO-Mk3.6.0; GFDL-ESM2M; HadGEM2-ES; ICHEC-EC-EARTH; IPSL-CM5A-MR; MIROC5; MPI-ESM-LR; NorESM1-M

TABLE 1. (*Continued*)

CORDEX region	RCM	GCM
C-SEA (Southeast Asia)	—	—
C-WAS (West Asia)	MPI-CSC-REMO2009 SMHI-RCA4	MPI-ESM-LR CanESM2; CNRM-CM5; CSIRO-Mk3.6.0; GFDL-ESM2M; HadGEM2-ES; ICHEC-EC-EARTH; IPSL-CM5A-MR; MIROC5; MPI-ESM-LR; NorESM1-M
C-GLOB (Global 50 km)	CSIRO-CCAM	ACCESS-1.0; CCSM4; GFDL CM3; CNRM-CM5; MPI-ESM-LR; NorESM1-M

precipitation (P) and minimum and maximum temperatures (T_N and T_X) from 1981–2100, for both RCP4.5 and RCP8.5, were considered. Unfortunately, we could not extend our analyses to RCP2.6 because, at the time of inquiry, the corresponding simulations did not cover the entire world. The selected spatial resolution is 0.44° (~50 km), as higher-resolution data (0.11° or 0.22°) are not available for all domains.

The primary sources of CORDEX data are the Earth System Grid Federation (ESGF) web portals. However, not every CORDEX simulation used in this study was available on the ESGF portal at the beginning of our data search. In the meantime, new simulations have been added to the ESGF data catalogue, but some areas are still covered by only a few simulations. Consequently, we obtained as yet unpublished data directly from the contact points for each domain. In total, we collected 103 GCM–RCM simulations. Those provided for the CORDEX domain Australia (AUS) are included in those provided at global scale by the Commonwealth Scientific and Industrial Research Organization (CSIRO). Unfortunately, no simulations for Southeast Asia (SEA) could be obtained. However, those belonging to East Asia (EAS) also include SEA in the domain.

The complete list of GCMs and RCMs related to the 103 simulations is reported in Table 1 and the responsible institute and key references in Table 2. The exceptionally large number of simulations used makes this study unique, and particularly valuable. Nonetheless, it must be pointed out that, as the number of simulations varies from region to region, the robustness of the results may be affected over regions where the number of simulations is limited (see section 3). Figure 1 shows the number of simulations per region, with the smallest number (<10) over Australia and southern Siberia, and the largest (>60) over the eastern Mediterranean region, where many CORDEX domains overlap.

In general, any procedure of subselecting models potentially introduces bias, so the use of varying number of simulations in different regions needs validation. Unfortunately (see Table 1), no simulations generated by the same combination of GCMs and RCMs are available over all the CORDEX domains, with the exception of the six GCMs coupled with the CSIRO-CCAM. Thus, performing a validation by comparing drought projections obtained using all 103 simulations versus those obtained using a combination of models based on a single RCM is likely to be depending too much on that single RCM. However, as discussed in section 3, the absence of clear discontinuities over the bordering areas between CORDEX domains suggests that the spatial distribution of the future drought conditions is not biased by using of different simulations over different regions.

Independently for each simulation, we computed drought indicators and derived drought variables, based on temperature and precipitation data, and (only at a later stage) the 103 outputs were merged over a common grid. Generally, the use of a large number of simulations avoided pronounced discrepancies along the borders of CORDEX domains, where simulations for different domains overlap. Over all domain borders, we tested whether the use of simulations from only one domain would give substantially different results compared with simulations from another domain. In only two cases, non-negligible discrepancies were found: along the Urals (borders between the Europe, central Asia, and Arctic domains) and, to a minor extent, southeastern China (borders between the central Asia, South Asia, and East Asia domains). Eventually, over these areas—as in all other areas—we elected to use the ensemble median of all simulations, in order to maintain methodological homogeneity with the rest of the global areas. See section 3 for details.

b. Meteorological drought indicators: SPI and SPEI

For each simulation, we converted the daily data into monthly averages for minimum and maximum temperature, and monthly sums for precipitation. As all

TABLE 2. GCMs and the RCMs used in this study, institute(s) owning the intellectual property, and key reference(s).

Type	Name	Institute	Reference(s)
GCM	ACCESS-1.0	CAWCR (Collaboration for Australian Weather and Climate Research) CSIRO (Commonwealth Scientific and Industrial Research Organization; Australia) BOM (The Australian Bureau of Meteorology, Australia)	Bi et al. (2013) Ackerley and Dommenget (2016)
GCM	CanESM2	CCCma (Canadian Centre for Climate Modeling and Analysis, Victoria, BC, Canada)	Chylek et al. (2011)
GCM	CCSM4	NCAR (National Center for Atmospheric Research, Boulder, Colorado, United States)	Gent et al. 2011
GCM	CESM1	NCAR	Meehl et al. 2013
GCM	CNRM-CM5	CNRM (Centre National de Recherches Météorologiques, Paris, France)	Voldoire et al. 2013
GCM	CSIRO-Mk3.6.0	CSIRO	Jeffrey et al. 2013
GCM	CMCC-CM	CMCC (Centro Euro-Mediterraneo per I Cambiamenti Climatici, Lecce, Italy)	Scoccimarro et al. 2011
GCM	GFDL CM3	NOAA (National Oceanic and Atmospheric Administration, United States)	Donner et al. 2011
GCM	GFDL-ESM2M	GFDL (Geophysical Fluid Dynamics Laboratory, Princeton, New Jersey, United States)	Dunne et al. 2012, 2013
GCM	HadGEM2-ES	MOHC (Met Office Hadley Centre for Climate Science and Services, Exeter, United Kingdom)	Collins et al. 2011
GCM	ICHEC-EC-EARTH	EC-EARTH Consortium, Europe	Koenigk et al. 2013 Hazeleger et al. 2010
GCM	IPSL-CM5A-MR	IPSL (Institut Pierre-Simon-Laplace, France) Universitè Pierre et Marie Curie (Paris, France) Universitè Pierre et Marie Curie (Paris, France)	Dufresne et al. 2013
GCM	MIROC5	Centre for Climate System Research (Kashiwa, Japan) Atmosphere and Ocean Research Institute, The University of Tokyo, (Kashiwa, Japan)	Watanabe et al. 2010.
GCM	MPI-ESM-LR	MPI (Max Planck Institute, Hamburg, Germany)	Giorgetta et al. 2013
GCM	MPI-ESM-MR		
GCM	NorESM1-M	NCC (Norwegian Climate Center and University of Bergen, Norway)	Bentsen et al. 2013
RCM	CCCma-CanRCM4	CCCma	Scinocca et al. 2016
RCM	CLMcom-CCLM4.8-17	CLM (Climate Limited-area Modeling) Community. Contributions by:	Rockel et al. 2008
RCM	CLMcom-CCLM4.8-17-CLM3.5	BTU (Brandenburg University of Technology, Cottbus, Germany);	Dosio et al. 2015
RCM	CLMcom-CCLM4–8-19	DWD (German Weather Service, Offenbach, Germany)	Smiatek et al. 2016
RCM	CLMcom-CCLM5.0.2	ETHZ (Swiss Federal Institute of Technology Zurich, ETH Zürich) UCD (University College Dublin, Ireland); WEGC (Wegener Center for Climate and Global Change, University of Graz, Austria)	
RCM	CNRM-ALADIN52	CNRM	Spiridonov et al. 2005
RCM	CNRM-ALADIN53	Météo-France (Paris, France)	Lucas-Picher et al. 2013 Tramblay et al. 2013
RCM	CSC-GERICS REMO2009	CSC-GERICS (Helmholtz-Zentrum Geesthacht, Climate Service Center, Hamburg, Germany) MPI	Teichmann et al. 2013 Jacob et al. 2012
RCM	CSIRO-CCAM	CSIRO	McGregor and Dix 2008
RCM	CYI-WRF351F	CYI-EEWRC (The Cyprus Institute, Energy Environment and Water Research Center, Nicosia, Cyprus	Zittis et al. 2014
RCM	DMI-HIRHAM5	DMI (Danish Meteorological Institute, Copenhagen, Denmark)	Christensen et al. 2006
RCM	MOHC-HadGEM3-RA	MOHC	Hewitt et al. 2011
RCM	ICTP-RegCM4–3	ICTP (Abdus Salam International Centre for Theoretical Physics, Trieste, Italy)	Giorgi et al. 2014

TABLE 2. (*Continued*)

Type	Name	Institute	Reference(s)
			Llopart et al. 2014
			Ozturk et al. 2017
RCM	IPSL-INERIS-WRF331F	IPSL INERIS (Institut National de l'Environnement Industriel et des Risques, Paris, France)	Menut et al. 2012
RCM	KNMI-RACMO21P	KNMI (Royal Netherlands Meteorological Institute, De Bilt, Netherlands)	van Meijgaard et al. 2008
RCM	KNMI-RACMO22E		
RCM	KNMI-RACMO22T		
RCM	SMHI-RCA4	SMHI (Swedish Meteorological and Hydrological Institute, Norrkoping, Sweden)	Samuelsson et al. 2015
			Strandberg et al. 2015
RCM	SMHI-RCA4-GUESS	University of Lund (Sweden)	Zhang et al. 2014
RCM	UQAM-CRCM5	UQAM (Université du Quebec à Montreal, Canada)	Šeparović et al. 2013 Diro et al. 2014

simulations are compliant with CORDEX standards, no gaps or spurious data were found, except for very few cases of unrealistically extremely low winter minimum temperature over northeastern Siberia in one of the simulations—which we nevertheless decided to retain. In fact, as our analyses is based on median values from all simulations available for a certain grid point, large outliers are excluded.

Estimating potential evapotranspiration (PET) in an environment with a changing atmospheric CO_2 concentration is not straightforward (Roderick et al. 2015; Milly and Dunne 2016). We used the Hargreaves–Samani equation (H-S; Hargreaves and Samani 1985), which derives PET by estimating solar radiation from minimum and maximum temperature and is frequently used in drought studies (e.g., Vangelis et al. 2011; Vicente-Serrano et al. 2011). The use of both minimum and maximum temperature avoids the large overestimation of droughts in dry and hot periods by models based on mean temperature only, as the Thornthwaite's model (Th; Thornthwaite 1948; Weiß and Menzel 2008; Shahidian et al. 2012). On the other hand, the H-S method tends to overestimate PET in humid regions and underestimate it in regions with high wind speed (Temesgen et al. 1999). The H-S method uses extraterrestrial radiation rather than solar radiation and neglects atmospheric transmissivity, which is influenced by high moisture content in the atmosphere in humid regions. Moreover, the

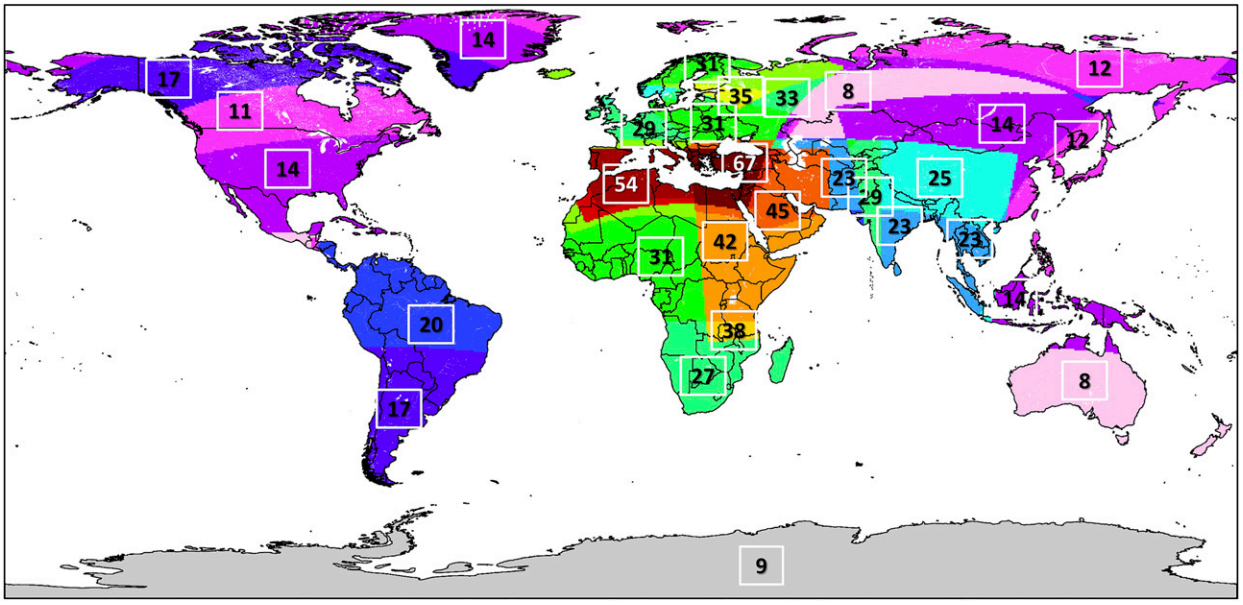

FIG. 1. Number of CORDEX simulations used. The numbers are valid for both RCP4.5 and RCP8.5.

H-S method does not consider atmospheric moisture, which is particularly important in humid regions, where PET tends to decrease as atmospheric moisture increases (McKenney and Rosenberg 1993; Tabari 2010).

More realistic estimations of PET, suitable for drought-related studies (Sheffield et al. 2012; Trenberth et al. 2014; Dai and Zhao 2017), could be obtained with the Penman–Monteith method (P-M; Allen et al. 2006). For example, Hosseinzadehtalaei et al. (2017) found smaller bias in future PET changes with the P-M method compared to the H-S method. In spite of this shortcoming, P-M is considered more realistic because is based on sunshine duration, temperature, vapor pressure, humidity, and wind speed data. However, it makes use of questionable physical assumptions, as its parameterization refers to a surface of grass with a sufficient amount of water; therefore, in very or extremely dry periods P-M tends to overestimate PET (Brutsaert and Parlange 1998). Unfortunately, such variables are available only for a limited number of CORDEX simulations, which is why we opted for H-S to compute PET, as was done in Spinoni et al. (2018) for Europe.

For each simulation, climate scenario, and grid point, we computed time series of SPI and SPEI values. Following McKee et al. (1993) for SPI and Vicente-Serrano et al. (2010) for SPEI, we fitted precipitation data on a gamma distribution to obtain SPI, and the difference between precipitation and PET on a log-logistic distribution to obtain SPEI.

The time scale of the drought indicator is sometimes used to define the type of drought, especially when the study focuses on drought impacts; that is, short scales (up to 3 months) refer to meteorological droughts, medium scales (6 months) to agricultural droughts, and longer scales (12 months or more) to hydrological droughts (Heim 2002). Rather than this definition, in this study we investigated meteorological droughts as driven by meteorological variables (Mishra and Singh 2010, 2011) using two meteorological indicators (SPI-12 and SPEI-12), similar to Spinoni et al. (2018) for Europe. We used a 12-month accumulation period when computing drought indicators (SPI-12 and SPEI-12), this being a compromise between short time scales suitable to detect the specific time when a drought event occurs and long time scales suitable for multiannual cycles. The analyses on seasonal drought projections at different warming levels using shorter time scales (in particular the SPI-3 and the SPEI-3) are left to future research.

As discussed in previous studies using a similar methodology (Spinoni et al. 2015b, 2018), we selected the entire period (1981–2100) as a baseline period to fit the underlying distribution of the drought indicators. In fact, the choice of a shorter period, possibly characterized by frequent and severe droughts, could influence the indicator over the entire period, leading to underestimation of droughts in other periods, or vice versa. Moreover, the longer the baseline period, the more robust the standardized drought indicators (Wu et al. 2005). In contrast, if only the past decades are chosen as a reference period, the possible local acclimatization as the century progresses cannot be taken into account. In particular, using past data as a reference period to investigate future drought events might introduce bias, since ''normal'' conditions in the past may become anomalous in the future, so that events at the end of the twenty-first century could be unrealistically extreme. Note that the baseline period described above should not be confused with the reference period (1981–2010) used in comparing the projected drought quantities.

The SPI and SPEI results have been analyzed separately, as we specifically wanted to isolate the effect of temperature on meteorological drought projections. The role of temperature, which is often incorporated in drought studies as PET, is critical and much debated in the scientific literature (Dai et al. 2018), due to the fact that, in the context of progressive warming, an increase of precipitation can be outbalanced by a larger atmospheric evaporative demand forced by higher temperatures. By separating the projected changes in drought variables according to the SPI and SPEI indicators, we have been able to analyze whether or not, and where, projected changes in precipitation and/or temperature drive future changes in drought frequency and severity. Furthermore, meteorological drought impacts can be better correlated with SPI or SPEI, depending on the socioeconomic sector involved (Naumann et al. 2015), and therefore different users can benefit from this study if the results for both indicators are presented separately.

c. *Drought frequency, severity, and extreme events*

Once we had computed time series, from 1981 to 2100, for the SPI-12 and SPEI-12 values at gridpoint scale (0.44°), for all simulations and both RCPs, we applied the same methodology as described in Spinoni et al. (2014) to detect drought events, that is, using the ''run theory'' as proposed by Yevjevich (1967). That is to say: a drought event starts when the drought indicator falls below one negative standard deviation for at least two consecutive months and ends when the indicator turns positive.

Drought frequency (DF) is then defined as the number of events in a given period, with the two investigated 30-yr periods in this study being 1981–2010 (representing the reference period) and 2071–2100 (representing the far future). The severity of an event is estimated as the sum, in absolute values, of all the monthly indicator values between the start and the end of the event. Since

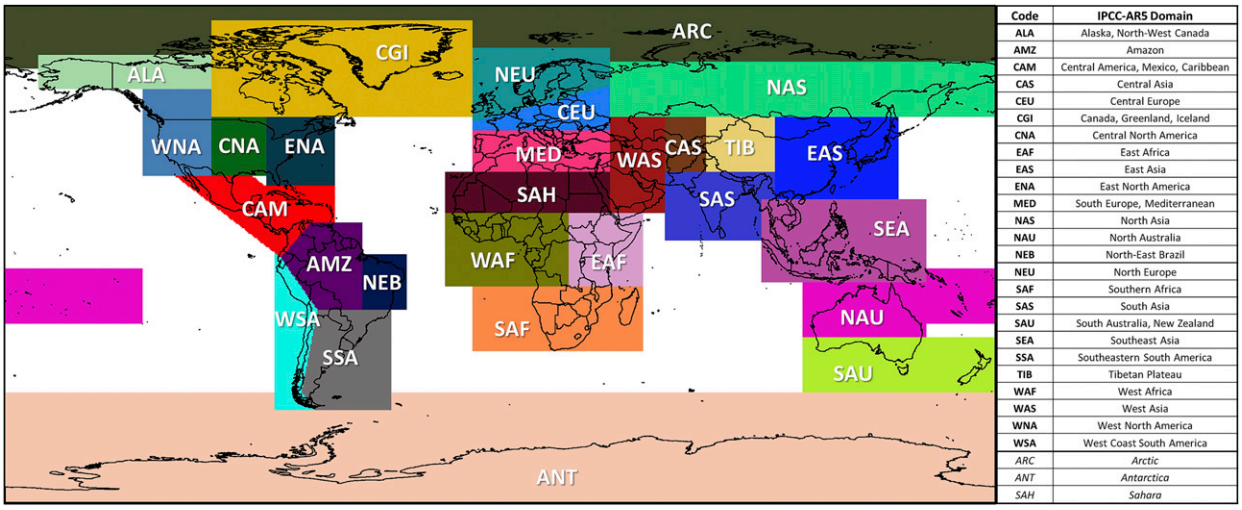

Code	IPCC-AR5 Domain
ALA	Alaska, North-West Canada
AMZ	Amazon
CAM	Central America, Mexico, Caribbean
CAS	Central Asia
CEU	Central Europe
CGI	Canada, Greenland, Iceland
CNA	Central North America
EAF	East Africa
EAS	East Asia
ENA	East North America
MED	South Europe, Mediterranean
NAS	North Asia
NAU	North Australia
NEB	North-East Brazil
NEU	North Europe
SAF	Southern Africa
SAS	South Asia
SAU	South Australia, New Zealand
SEA	Southeast Asia
SSA	Southeastern South America
TIB	Tibetan Plateau
WAF	West Africa
WAS	West Asia
WNA	West North America
WSA	West Coast South America
ARC	*Arctic*
ANT	*Antarctica*
SAH	*Sahara*

FIG. 2. Macroregions for the regional statistics. We adapted the IPCC Fifth Assessment Report official domains to our scopes. For three main regions (Arctic, Antarctica, and Sahara), we did not compute regional statistics.

our focus is on the change in severity of the average drought event between the two periods, here drought severity (DS) refers to the average severity—not the total severity—of drought events in the selected period. As the world is likely to face more extreme events during the twenty-first century (IPCC 2014), we defined a specific quantity (PK, for "peak events") representing the number of drought events during 2071–2100 that are more severe than the most severe event that occurred during 1981–2010.

In the maps included in this paper, the drought quantities are presented as the median values over all simulations available for the corresponding grid point. Thus all the available simulations for each point were used, as we prioritized maximum possible use of information. Using median values, together with the overall large number of simulations, helps to minimize the impact on the results of individual simulations, which may be biased and thus lead to biased SPI and SPEI time series. Over the borders between two CORDEX domains (regions), some model grids do not perfectly overlap (although the shift is in most cases less than 0.05°). Therefore, we interpolated the shifted simulations over a common 0.44° grid, using an interpolation scheme based on radial Gaussian weights. The only area where we found nonnegligible discontinuity between domains is over the Urals (Europe and central Asia).

The core results of this study focus on the changes in the selected drought variables between the reference period (1981–2010) and the far future (2071–2100). If not explicitly stated otherwise, such changes are considered robust in sign if at least two-thirds of the simulations indicate a change with the same sign. For instance, for a given grid point where 10 simulations are available, an increase in drought frequency is defined as robust in sign if at least seven simulations project an increase. We evaluated the possibility of using a larger threshold (e.g., 75% of model sign agreements), but the robustness in sign of the results was sensitive to outliers in regions where a very limited number of runs (<10) is available.

The results have also been analyzed at the macroregional scale, using the regions described in the Special Report of the IPCC "Managing the Risks of Extreme Events and Disasters to Advance Climate Change Adaptation" (IPCC 2012). However, as is evident in Fig. 2, we made some minor changes. The Caribbean islands and Central America form one region, as do the north tropical Pacific and northern Australia. We discarded the west Indian Ocean and southern and eastern tropical Pacific islands, due to the small fraction of land.

As in Spinoni et al. (2014) and Spinoni et al. (2018), we excluded from our analyses extremely arid or very cold areas, such as the Sahara and Antarctica. Areas excluded are those with a 30-yr (1981–2010) average annual ratio of precipitation to PET below 0.05 (arid), and with a similar 30-yr average annual PET below 365 mm (cold). These areas are not considered when showing global or macroregional percentage changes in areas affected by drought.

3. Results and discussion

a. Validation of drought projections: CORDEX data versus observed data

Before using the ensemble of CORDEX simulations to analyze drought projections, we tested their reliability versus observed data for 1981–2010 (the recent past). In the CORDEX simulations this period is a combination of

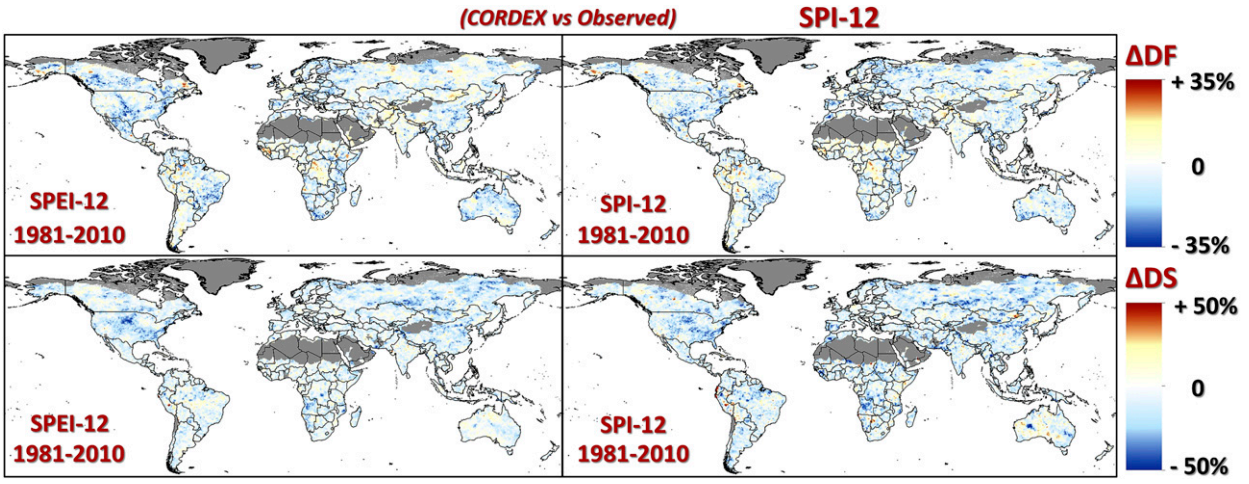

FIG. 3. Difference (Δ in %) of (top) drought frequency (DF) and (bottom) average severity of drought severity (DS) between CORDEX simulation data (*s*) and observed data from CRU and GPCC (*o*) for the period 1981–2010. Positive values mean that the CORDEX simulations overestimates observed values.

the historical experiments data (until 2005) and future projections data (2006–10, driven by the RCP). The observational datasets used for validation are the Global Precipitation Climatology Centre (GPCC, version 7) of the German Meteorological Office (DWD) (Schneider et al. 2008; Becker et al. 2013), and the Climate Research Unit Time series (CRUTS, version 4.01) of the University of East Anglia (Harris et al. 2014). We obtained precipitation data from GPCC and temperature data from CRUTS. Although CRUTS includes PET, computed based on the Penman–Monteith method, we used minimum and maximum temperature data to obtain PET based on the Hargreaves–Samani equation, and in turn, SPI and SPEI, to ensure homogeneity with the CORDEX outputs.

The drought variables selected for validation were drought frequency (DF) and drought severity (DS; averaged over events) during 1981–2010. The spatial resolution of the GPCC and CRUTS gridded data (0.5°) is slightly coarser than that of the CORDEX data (0.44°), so we interpolated DF and DS derived from the observational datasets over the CORDEX grid. We selected a kriging-based interpolation method (Cressie 1990) based on weighted Gaussian distance between points and a search radius of 75 km. The resulting error is likely to be negligible, as the difference in spatial resolution is small, and other sources of bias (e.g., low number of input stations in remote regions) can be more relevant.

Results show that CORDEX ensemble median values slightly underestimate both DF and DS, generally, when compared with the observational datasets (Fig. 3). Globally, the underestimation is larger for DF (about 12% for SPI and 11% for SPEI) and smaller for DS (about 10% for SPI and 8% for SPEI). However, for both drought variables (DF and DS) and indicators (SPI and SPEI), more than 50% of the land areas show differences smaller than 5%. Locally, regions where the underestimation is largest (on average close to 15%) are visible over the central United States, northwestern Mexico, and western Canada (for DF), as well as Angola and the mountainous regions of central Asia (for DS). In contrast, the largest overestimation (about 10%) by CORDEX simulations is visible, locally, over the Democratic Republic of Congo (for DF) and Australia (for DS based on SPI).

While the discussed discrepancies do not directly affect the results shown in the following sections, the validation exercise is useful to investigate for which regions the CORDEX simulations are more or less reliable. Although the ensemble median does not show excessively large discrepancies, individual ensemble members may have larger errors. During the first phase of testing, we tested the reliability of single-model runs by applying a bootstrapping technique to the ensemble: we defined a criterion for excluding a simulation if it showed drought frequency (over 1981–2010 and based on SPEI) with an absolute difference versus the observational datasets of more than three events per 10 years, and covering more than 66% of its domain. This never occurred for the 103 simulations used in this study, although a couple did show discrepancies above the threshold for large areas of Siberia.

b. *The twenty-first century: A drying or wetting warming?*

Climate simulations are in agreement regarding a warming world during the twenty-first century (Meehl et al. 2007; IPCC 2014); therefore, we can expect a global increase in PET driven by temperature. An increase in

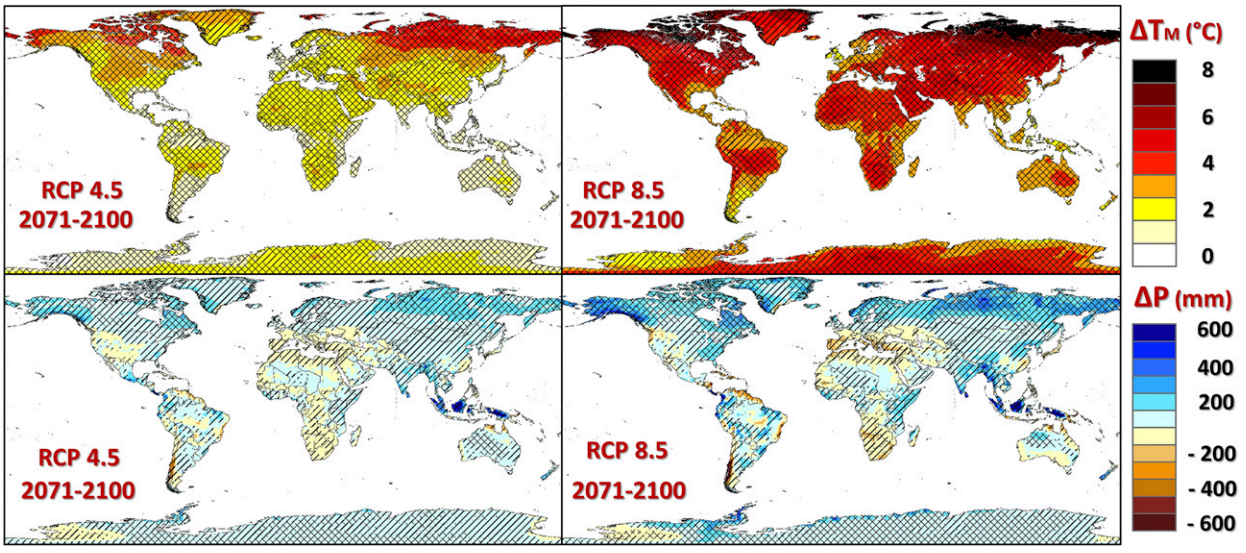

FIG. 4. Mean temperature (T_M) and annual precipitation (P) change between 1981–2010 and 2071–2100 under (left) RCP4.5 and (right) RCP8.5 using CORDEX simulations. The change is robust in sign if more than two-thirds of the simulations agree on the sign of change. It is robust in magnitude if the median change (based on the ensemble) between 1981–2010 and 2071–2100 is larger than the intermodel variability (one standard deviation) of the 30-yr average value over 1981–2010. Cross-hatched lines represent a change robust in both magnitude and sign, hatched lines (////) represent change robust in sign only, hatched lines (\\\\) represent change robust in magnitude only (extremely rare), and areas with no hatched lines represent change not robust neither in magnitude, nor in sign.

evaporative demand, however, does not per se result in an intensification of drought frequency and/or severity. Only the combined effect of changes in both rainfall and PET will determine where droughts become more or less frequent and severe.

Figure 4 shows the change in the ensemble median of mean temperature (T_M) and total precipitation (P) between the end of the twenty-first century and the reference period. The upper panels show that, under both climate scenarios, the overall increase in mean temperature is robust in both magnitude and sign over the vast majority of land areas. Precipitation is projected to increase or decrease depending on the region and scenario, showing larger spatial and temporal variability and, in general, a wetting or drying tendency for RCP4.5 corresponds to a stronger wetting or drying tendency for RCP8.5. In particular, the increase is robust in both sign and magnitude over northern latitudes, central Australia, and Antarctica, whereas over the eastern United States, the Horn of Africa, India, most of China, and southeastern Asia most models agree on the sign of the change, but not necessarily on its magnitude. On the contrary, a drying that is robust in sign is projected for the Mediterranean and South Africa, parts of Mexico and southern Argentina, and eastern China, especially under RCP4.5. However, over most of central and western United States, Mexico, South America, central Europe, and Africa the change in precipitation is not robust, either in sign or magnitude (e.g., see Dosio et al. 2019). However, the Amazon subdomain is a special case, once it is a large region that includes more biomes than only Amazon tropical forest. For this reason, in further studies this subdomain may be split into minor regions, to investigate whether more robust local precipitation trends could be expected.

Although the main scope of this study is to investigate changes in drought frequency and severity, and not in temperature and precipitation per se, Fig. 4 represents the first map of its kind (to our knowledge) to show global temperature and precipitation projections based on a large ensemble of RCMs at a high spatial resolution (0.44°). Temperature projections shown in Fig. 4 agree with those reported in the latest IPCC Assessment Report (IPCC 2014), based on global simulations from the phase 5 of the Coupled Model Intercomparison Project (CMIP5) (Taylor et al. 2012) and with the previous set of simulations from CMIP3 (Knutti and Sedláček 2013). As shown for example by Dosio (2017) for Africa, RCM projections for temperature largely agree with those of the driving GCMs. For precipitation, there are numerous areas with an uncertain change, in line with previously published GCM-based precipitation projections (Power et al. 2012; Knutti and Sedláček 2013; IPCC 2014), but uncertainties may be reduced by using constrained or weighted GCM ensembles, as done in Mexico and Central America (Colorado-Ruiz et al. 2018) and in the Arctic (Knutti et al. 2017). In general both GCM- and

TABLE 3. Average mean temperature (ΔT_M) and precipitation (ΔP) differences between 1981–2010 and 2071–2100 under the RCP4.5 and the RCP8.5 for 28 macroregions and at global scale (only over land). The last two columns show the percentage of areas in which precipitation is projected to increase. The regions with an increase or decrease in precipitation larger than 10% are highlighted in bold.

	RCP4.5	RCP8.5	RCP4.5	RCP4.5	RCP8.5	RCP8.5	RCP4.5	RCP8.5
Region	ΔT_M (°C)		ΔP (mm)	ΔP (%)	ΔP (mm)	ΔP (%)	$\Delta P > 0$ (% area)	
ALA	3.7	6.9	**210.2**	**58.6**	**101**	**28.1**	100.0	100.0
CGI	3.9	6.6	**160.8**	**32.8**	**99.7**	**20.3**	99.5	99.5
WNA	2.9	5.1	27.6	5.5	18	3.6	55.5	63.7
CNA	2.8	4.7	54.3	6.4	16.7	2.0	65.2	88.4
ENA	2.8	4.9	**115.3**	**10.6**	59	5.4	98.3	99.8
CAM	2.0	3.9	52.2	3.7	81.9	5.8	76.0	63.2
AMZ	2.2	4.2	30.3	1.4	14.6	0.7	64.5	69.4
NEB	2.2	4.2	52.5	4.4	37.1	3.1	67.1	68.5
WSA	2.2	4.2	**−87.5**	**−10.9**	−54.9	−6.9	33.6	33.6
SSA	1.9	3.6	46.5	4.7	29.8	3.0	75.5	70.8
NEU	2.3	4.1	**140.2**	**18.4**	**77.3**	**10.1**	95.9	97.7
CEU	2.3	4.2	13.7	1.9	13.3	1.9	61.3	53.9
MED	2.3	4.5	**−78.2**	**−17.7**	−34.5	−7.8	5.0	1.3
SAH	2.5	4.8	4.5	6.8	2.4	3.6	49.3	57.3
WAF	2.2	4.1	22.7	1.9	3.1	0.3	48.2	62.5
EAF	2.1	4.0	71.0	8.2	33.0	3.8	77.1	84.8
SAF	2.4	4.6	−44.3	−6.1	−20.3	−2.8	23.0	19.1
NAS	4.1	6.7	**147.4**	**34.0**	**93.7**	**21.6**	99.1	98.3
WAS	2.9	5.3	−3.5	−1.6	−1.8	−0.8	50.8	50.9
CAS	3.0	5.4	14.7	5.3	8.5	3.1	69.1	71.4
TIB	2.7	5.3	**60.4**	**25.1**	**32.8**	**13.6**	95.1	96.4
EAS	2.5	4.6	57.5	7.2	41.3	5.2	83.3	80.9
SAS	2.2	4.3	**130.0**	**11.2**	80.7	7.0	88.3	89.4
SEA	1.6	3.2	249.8	9.8	228.7	9.0	82.1	77.9
NAU	1.8	3.7	19.9	4.0	25.2	5.1	84.3	69.9
SAU	1.8	3.5	4.8	0.9	36.7	6.5	92.1	34.2
ANT	2.0	4.1	**50.0**	**24.1**	**22.2**	**10.7**	92.7	93.4
ARC	5.1	8.4	**209.6**	**87.9**	**124**	**52.0**	100.0	100.0
GLOBE	**2.6**	**4.8**	**59.6**	**8.1**	**38.6**	**5.2**	**72.9**	**73.4**

CORDEX-based results show overall similar spatial patterns, especially the drying tendency over Chile, the Mediterranean region, and southern Africa (e.g., Dosio et al. 2019).

Table 3 (which refers to the same acronyms as in Fig. 2) summarizes the projected temperature and precipitation changes between 1981–2010 and 2071–2100 at macroregional scale. Over land, the global average temperature increase by the end of the twenty-first century is estimated at 2.6°C for RCP4.5 and at 4.8°C for RCP8.5, being most extreme over the Arctic region (ARC) and least extreme over southern South America (SSA). At global scale, annual precipitation is projected to increase, on average, by approximately 8% for RCP4.5 and 5% for RCP8.5. For both climate scenarios, approximately 73% of the lands will face an increase in precipitation by the end of the twenty-first century (Table 3). The fraction of land area projected to become wetter is particularly small for two macroregions, the Mediterranean region (MED; i.e., 5% for RCP4.5 and 1.3% for RCP8.5) and southern Africa (SAF; 23% for RCP4.5 and 19.1% for RCP8.5), in agreement with the drying tendency discussed previously. Finally, southern Australia (SAU) shows the largest difference between precipitation projection depending on the underlying RCP, with the fraction of land projected to become wetter under RCP4.5 (i.e., 92.1%) greatly reducing under RCP8.5 (i.e., 34.1%).

c. *Drought frequency, severity, and extreme droughts projections*

Before analyzing the drought projections for the RCMs, it is interesting to briefly discuss those obtained by the driving GCMs. Figure 5 shows the changes in drought frequency (DF; events per decade) and average severity of drought events (DS; average severity per decade) between the reference period (1981–2010) and the far future (2071–2100) under the RCP4.5 and the RCP8.5. As input data, we used the ensemble median of 16 GCMs (see Table 1), regridded at medium spatial resolution (1.8°). The choice of such common resolution depends on the optimal choice between the single resolutions (from 0.75° × 0.75° to 2.5° × 2°).

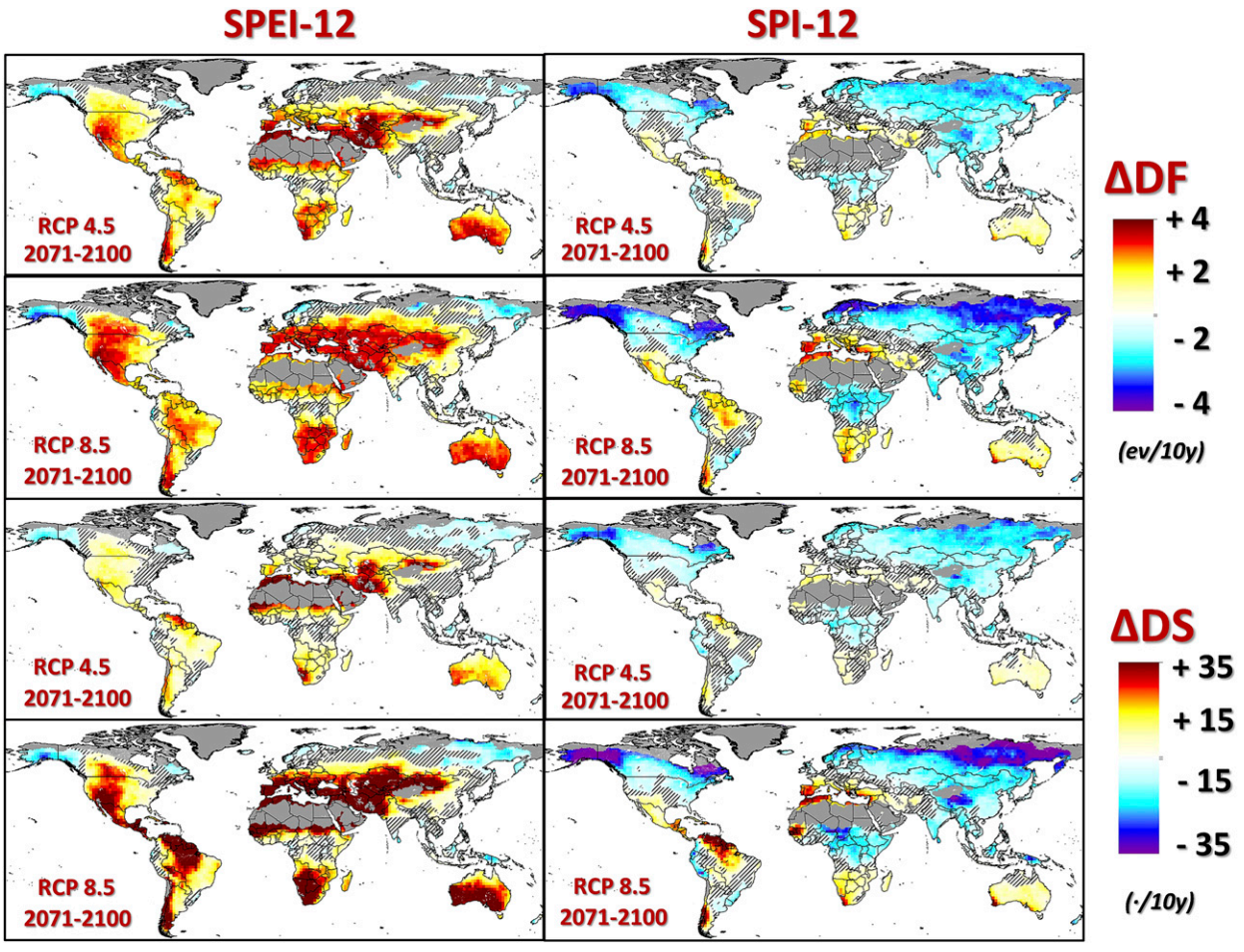

FIG. 5. Differences in drought frequency (DF; events per decade) and average severity of events (DS; severity per decade) between 2071–2100 and reference period (1981–2010) under the RCP4.5 and the RCP8.5. As input, we used the 16 GCMs (see Table 1) regridded over the common spatial resolution of 1.8°. Very cold and desert areas have been masked. Hatched lines correspond to areas where less than two-thirds of simulations agree on the sign of change. Note that the hatched lines represent different features than Fig. 4.

The same interpolation scheme used for regridding the CORDEX simulation was used.

Figure 5 shows some clear spatial patterns: the drought frequency and severity are projected to increase in much larger areas according to the SPEI than to the SPI, although they agree about the increase of both quantities (under both scenarios) over the Amazon forest, southern South America, the Mediterranean region, southern Africa, and southern Australia. According to the SPI, most of the areas at high latitudes are projected to see a decrease in both drought frequency and severity. The areas where less than two-thirds of the simulations agree on the sign of change are different according to the SPEI (medium high latitudes in Northern Hemisphere and equatorial Africa) and the SPI (central Europe, the Middle East, and parts of Brazil).

The same analyses were repeated using the 103 CORDEX simulations, improving the spatial resolution from 1.8° to 0.44°. Figure 6 shows the changes in DF: as expected, the area projected to experience more drought events in the future is much larger according to SPEI (approximately 72% for both RCPs) than with SPI (approximately 17% for RCP4.5 and 16% for RCP8.5). The corresponding values per macroregion are reported in Table 4. The two indicators agree on the projected decrease in DF over high latitudes and southeastern Asia and on the increase over the Mediterranean region, Chile and Argentina, southern Africa, and southeastern China. Areas where the change is not robust in sign show some differences. The projected change is not robust in sign over India for SPEI, while it is robust in sign for SPI. On the contrary, over the U.S. Midwest, northwestern Mexico, central Europe, and tropical Africa the projected change is robust in sign for SPEI and not for SPI. Some regions (Table 4) show opposite tendencies, in particular under the RCP8.5. Examples are eastern

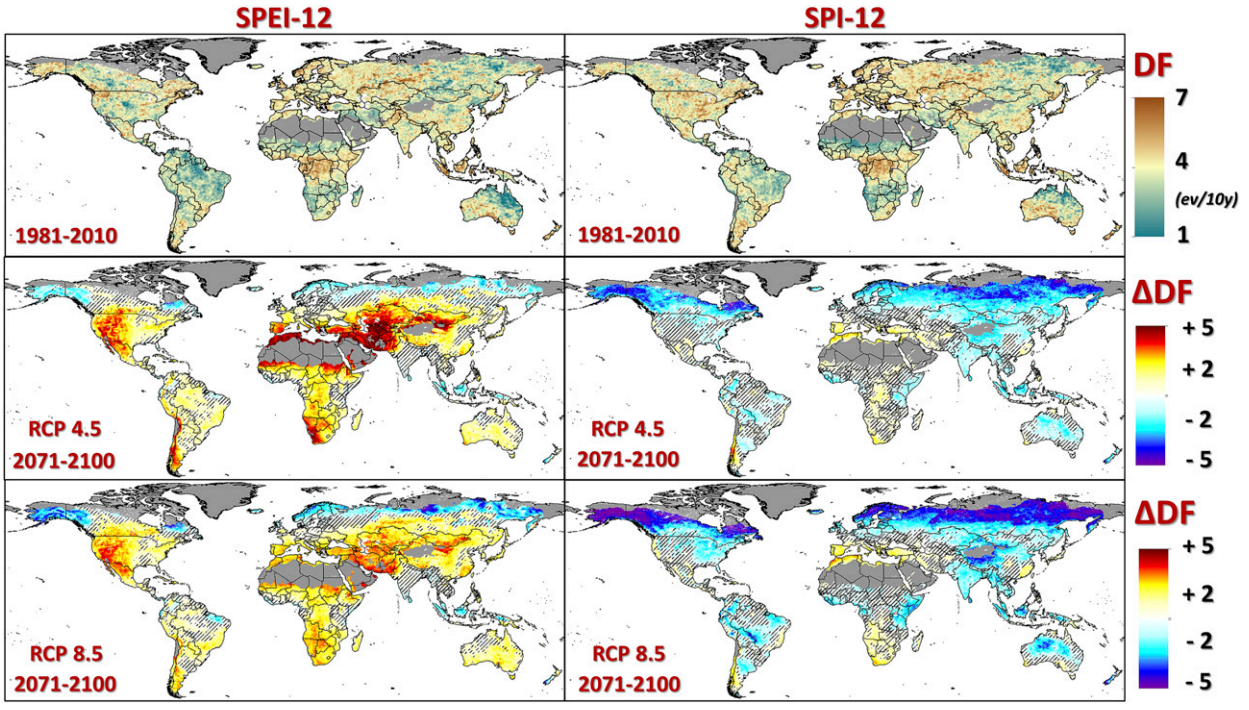

FIG. 6. (top) Drought frequency (DF; events per decade) in 1981–2010. (middle),(bottom) Difference between drought frequency in 2071–2100 and drought frequency in 1981–2010, under RCP4.5 and RCP8.5, respectively. The maps show the ensemble median values obtained using all the CORDEX simulations available for each grid point. Very cold and desert areas have been masked. Hatched lines correspond to areas where the change is uncertain, that is, where less than two-thirds of simulations agree on the sign of change. Note that the hatched lines represent different features than in Fig. 4.

North America, Amazonia (under RCP8.5 only), the Horn of Africa, central Asia, and central Australia, mainly due to the nonrobust precipitation changes over those areas.

In general, the two scenarios agree on the sign of change between the recent past and far future for each of the indicators. For SPI, the change in DF under RCP8.5 is in general larger than that under RCP4.5. However, SPEI shows a larger increase in DF under RCP4.5 compared with RCP8.5 especially for the Mediterranean region, most of central Asia, and Africa. A possible explanation for this somewhat counterintuitive result can be given by combining the information from Fig. 6 (frequency; see also Fig. 7 for validation) and Fig. 8 (severity, which is linked to drought duration). In fact, over these areas, under RCP8.5, the length of the droughts is projected to increase enormously (with some droughts lasting for several years) with the result that their frequency is reduced. This hypothesis is confirmed by analyzing the changes in drought duration (for SPEI): over 97.3% of the mentioned areas, droughts are projected to last much longer under RCP8.5 than RCP4.5 (not shown). Under the moderate scenario the droughts are projected to be more frequent than in recent past, but the increase in severity and duration will be smaller than under the more extreme scenario.

The spatial patterns of the driving GCMs are in general similar to those of the RCMs, but with the use of RCMs some different patterns are found. First, the projected increase of drought frequency is smaller (according to CORDEX) over Australia, where the SPI projects a decrease in central territories. Second, two areas (India for the SPEI and tropical Africa for the SPI) show not robust (in sign) changes according to CORDEX simulations. Third, GCMs tend to generally overestimate the increase in DF under the RCP8.5 over Northern Hemisphere compared to the RCMs. This partly depends on the effect that a coarser resolution unavoidably introduces, but the use of RCMs (which account for regional physical features) becomes very useful to distinguish between regions with a moderate, large, or very large increase as it occurs in the western United States and central Asia. In fact, in Fig. 6 the borders between areas with progressively larger changes are better defined and the use of a larger number of simulations leads to more reliable delineation of areas with robust (in sign) changes.

Figures 6 and 8 show no clear discontinuities over borders between CORDEX domains, proving that the spatial patterns of the drought projections do not depend on the different set of simulations used in different regions. However, this is valid for the ensemble medians,

TABLE 4. Percentage of area in which drought frequency is projected to increase (decrease) from 1981–2010 to 2071–2100 under RCP4.5 and RCP8.5 and according to SPI-12 and SPEI-12. The change is uncertain (Unc) if less than two-thirds of simulations agree on the sign of change, otherwise ($\Delta DF > 0$ or $\Delta DF < 0$) more than two thirds of the model agree on the change in sign.

2071–2100 vs 1981–2010 Area (%)	RCP4.5						RCP8.5					
	SPI12			SPEI12			SPI12			SPEI12		
Region	ΔDF > 0	Unc	ΔDF < 0	ΔDF > 0	Unc	ΔDF < 0	ΔDF > 0	Unc	ΔDF < 0	ΔDF > 0	Unc	ΔDF < 0
ALA	0.0	0.0	100.0	12.4	18.4	69.2	0.0	0.0	100.0	6.2	16.4	77.4
CGI	0.2	4.0	95.8	43.2	23.2	33.6	0.0	1.8	98.2	52.5	15.2	32.4
WNA	11.7	36.4	51.8	81.4	12.7	5.9	15.1	30.3	54.6	88.5	6.7	4.8
CNA	12.2	34.2	53.5	92.8	6.4	0.7	8.4	23.7	68.0	91.2	8.8	0.0
ENA	2.2	18.1	79.7	79.8	16.8	3.4	0.0	4.8	95.2	86.1	13.0	1.0
CAM	34.5	50.0	15.5	77.6	16.7	5.7	36.1	41.6	22.3	74.7	16.4	8.9
AMZ	4.5	55.3	40.3	69.1	27.9	3.0	3.0	45.1	51.9	53.2	43.3	3.5
NEB	9.5	48.8	41.6	52.2	37.8	10.0	13.9	33.7	52.4	38.4	40.2	21.4
WSA	45.1	31.6	23.3	86.4	8.1	5.5	43.9	24.3	31.9	77.7	15.2	7.2
SSA	14.9	49.6	35.5	80.4	18.7	0.9	16.4	44.0	39.6	78.6	20.5	1.0
NEU	0.3	7.1	92.6	8.8	22.6	68.5	0.0	2.7	97.3	6.9	19.9	73.2
CEU	6.3	44.2	49.4	70.9	23.8	5.3	6.7	34.7	58.5	78.0	21.5	0.6
MED	88.2	11.5	0.3	99.9	0.1	0.0	97.0	3.0	0.0	100.0	0.0	0.0
WAF	32.7	47.3	20.0	87.7	8.4	3.9	13.7	49.2	37.1	86.6	9.1	4.3
EAF	19.3	37.2	43.5	78.2	18.5	3.3	4.6	39.6	55.7	74.7	21.1	4.1
SAF	50.0	48.6	1.4	98.6	1.4	0.0	72.4	25.2	2.4	98.5	1.5	0.0
NAS	0.0	2.4	97.6	47.6	22.1	30.3	0.0	2.5	97.4	52.8	14.3	32.9
WAS	50.3	41.1	8.6	100.0	0.0	0.0	40.8	52.0	7.2	100.0	0.0	0.0
CAS	22.3	36.1	41.6	100.0	0.0	0.0	12.4	38.6	48.9	100.0	0.0	0.0
TIB	0.8	4.6	94.6	97.8	2.2	0.0	0.3	5.7	93.9	97.9	2.1	0.0
EAS	10.0	30.8	59.2	83.3	16.5	0.2	13.5	29.4	57.1	92.3	7.7	0.0
SAS	1.1	12.1	86.8	32.2	53.7	14.1	1.0	9.3	89.7	34.9	50.4	14.7
SEA	10.3	25.1	64.6	29.7	32.5	37.7	11.4	23.2	65.4	23.0	43.5	33.4
NAU	8.0	24.0	68.0	75.0	20.5	4.6	7.6	20.5	71.9	72.1	26.1	1.8
SAU	10.5	39.5	50.0	83.7	10.7	5.6	30.3	38.9	30.7	91.4	4.1	4.5
GLO	16.9	30.6	52.5	72.1	17.3	10.6	16.1	26.4	57.5	71.7	17.2	11.1

while some discontinuities over bordering regions occur when computing the standard deviation of changes in drought frequency (Fig. 7), in particular over the Urals and, to lesser extent, over eastern China. Using the *best sample* [i.e., the eight simulations (eight is the minimum number of simulations over any area); see Fig. 1] with the smallest spread over each CORDEX domain, such discontinuities disappear.

Given the large number of simulations employed, one could expect a larger intersimulation spread (Fig. 7), but for DF it is smaller than 0.5 events per decade over most land areas. The areas with largest spread (and consequently less robust outputs in terms of magnitude) for the SPEI are eastern Canada, the Baltic republics, central Russia, India, and—for RCP8.5 only—the Horn of Africa and southeastern Asia. For the SPI, changes in DF under the RCP4.5 show no particular areas with large spread, whereas under RCP8.5 the spread is relevant for equatorial and tropical latitudes (i.e., areas with larger annual precipitation totals). However, for an ensemble of climate models, the geographical distribution of the uncertainties represented by model spread at the gridpoint scale could overestimate the projected range, leading to physically implausible patterns of change on global and regional scales, as climate change impacts will never be realized as the worst (or best) case everywhere (Madsen et al. 2017).

The changes in DS (see Fig. 8) are larger in percentage than those for DF. For SPEI, only latitudes higher than 55°N and southeastern Asia will face a decrease in DS. For SPI, on the other hand, southern Chile and Argentina, the Mediterranean region, large parts of southern Africa, and (under RCP8.5 only) southeastern China and southwestern Australia are projected to face an increase in DS. Moreover, the regions where the change is not robust in sign are larger for SPI than for SPEI, and consequently the areas with opposite robust tendencies in sign (i.e., increase for SPEI and decrease for SPI) are limited to central Asia and central Australia. The intersimulation spread for DS is spatially similar to that for DF (see Fig. 7), and thus we do not show the corresponding maps.

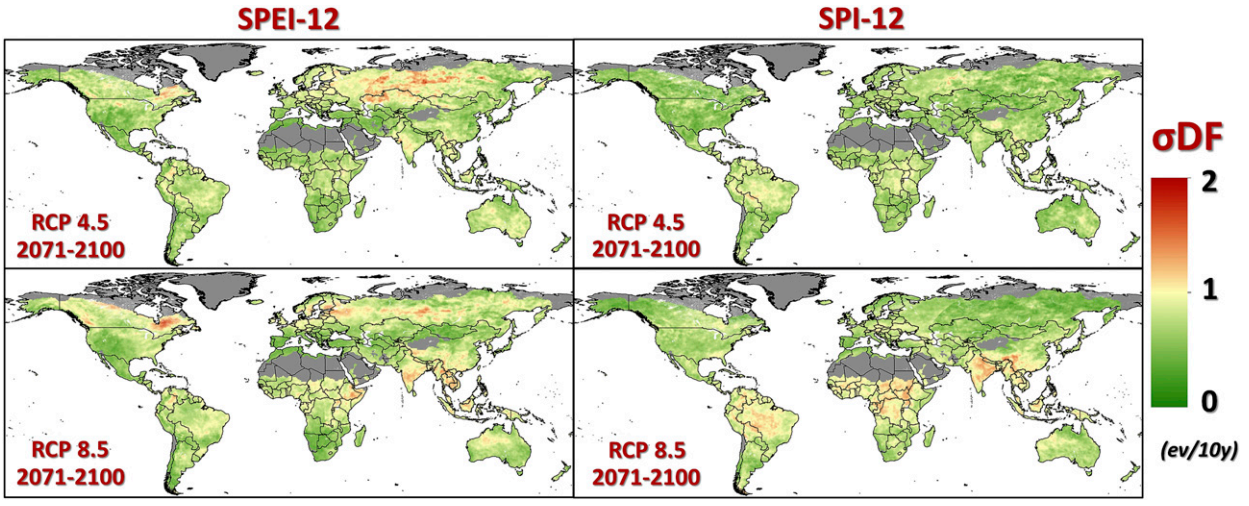

FIG. 7. Standard deviation of the ensemble median change in drought frequency (DF) using all the CORDEX simulations for each grid point. Very cold and desert areas have been masked.

For DS, the overall spatial patterns using GCMs only or the combinations of GCMs and RCMs are almost identical according to the SPEI, although under the RCP4.5 the use of RCMs makes a notable difference over western United States (Figs. 5 and 6). The projections of DS according to the SPI show remarkable differences under RCP8.5 over South America, where the use of RCMs turns positive changes into not robust in sign or even slightly negative changes in tropical South America, in agreement with the analyses of Llopart et al. (2014) and Sánchez et al. (2015), who showed that the downscaling RCMs can project a positive precipitation signal even though the

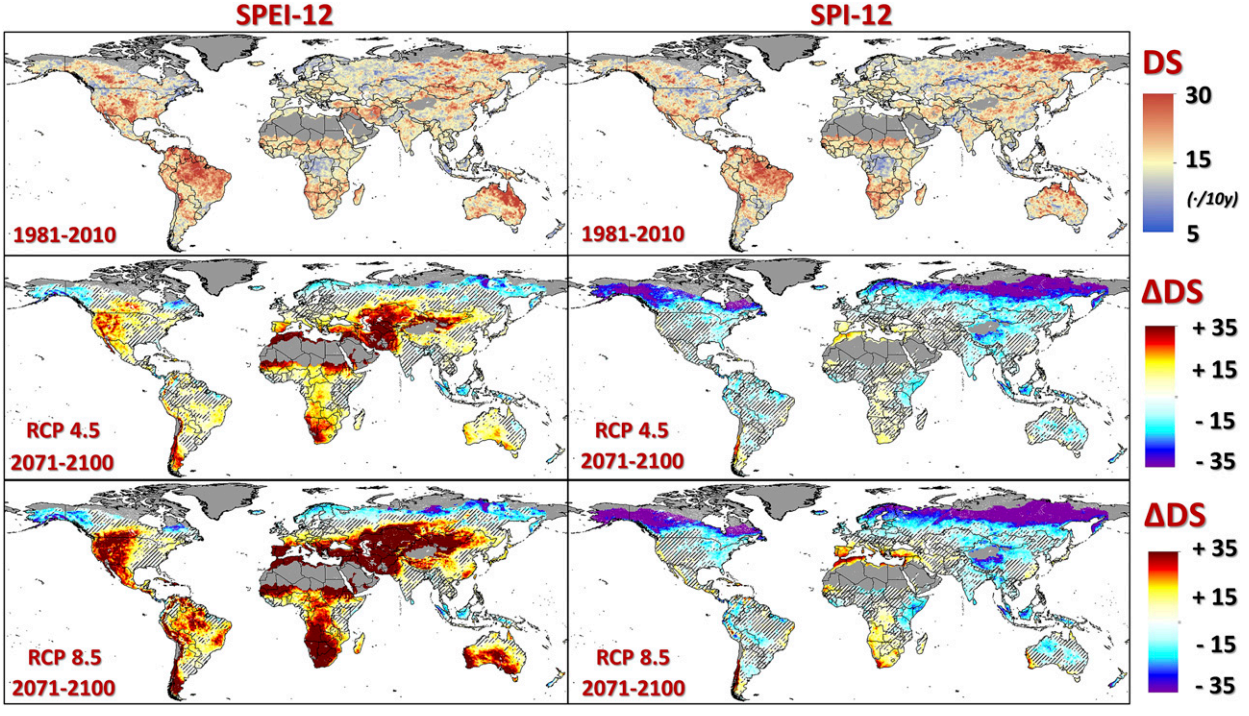

FIG. 8. As in Fig. 6, but shows the ensemble median severity of drought events (DS) and the corresponding changes. DS is the integral of all the negative values of the indicator during the drought event, in absolute values. Very cold and desert areas have been masked. Hatched lines correspond to areas in which less than two-thirds of simulations agree on the sign of change. Note that the hatched lines represent different features than in Fig. 4.

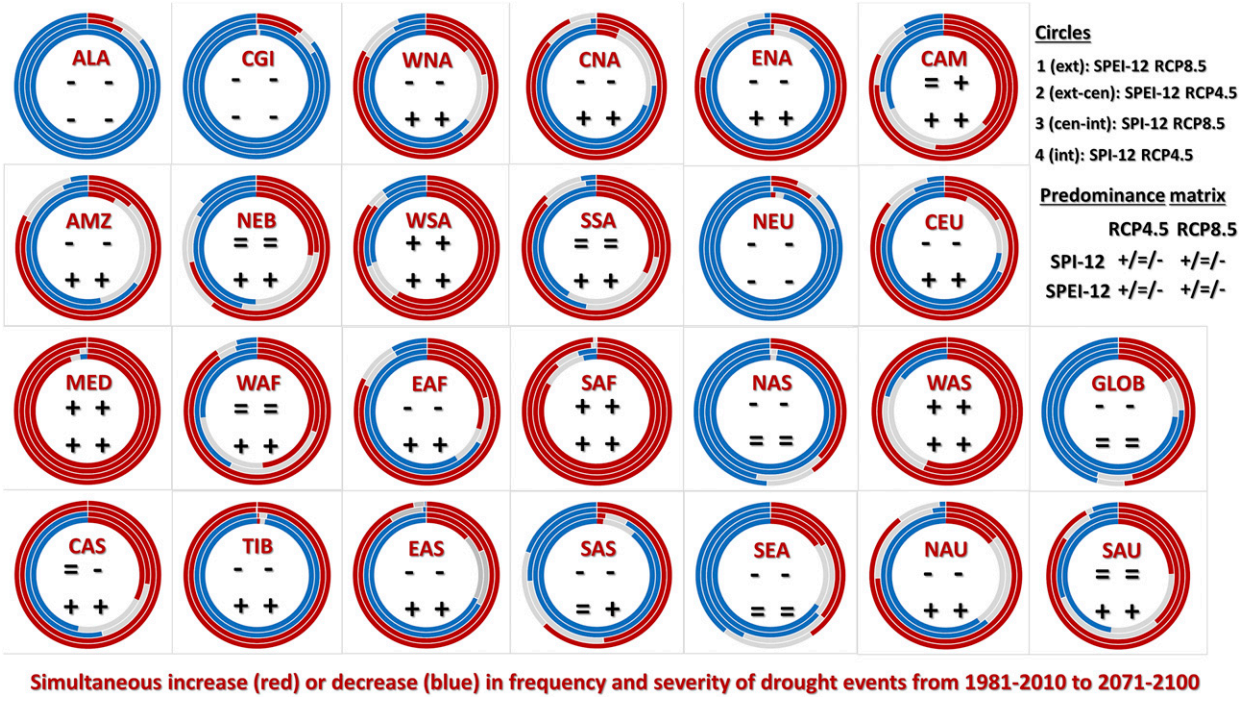

FIG. 9. Percentage of areas projected to experience an increase (red) or decrease (blue) in both drought frequency and severity from 1981–2010 to 2071–2100. Gray refers to either mixed or not robust changes. The inner circles refer to SPI-12 (internal: RCP4.5; central-internal: RCP8.5), the outer circles to SPEI-12 (central-external: RCP4.5; external: RCP8.5). The ''predominance matrix'' reports the dominant tendency: + (−) means that more than 50% of the areas show a simultaneous increase (decrease) in both DF and DS, = means that the simultaneous increase and decrease occurs in less than 50% of the areas.

driving GCMs show little or negative change. Moreover, under the RCP4.5, the decrease in DS at high latitudes in the Northern Hemisphere is larger according to the use of RCMs than to GCMs only. In general, the use of RCMs helps providing a better representation of areas with robust (in sign) changes according to the SPI in both hemispheres.

Based on Figs. 6 and 8 we can highlight regions where drought events are projected to be both more frequent and severe (Fig. 9). According to SPEI, most of the regions show a large fraction of area falling in this ''worst case'' situation, while for SPI this happens for only a few regions, in particular the Mediterranean region and southern Africa. Over the Tibetan Plateau, the two indicators completely diverge, although results for this region may be largely influenced by its complex orography. In addition, this region contains the smallest number of grid points used for the analysis, due to the masking of very cold high-elevation areas. At a global scale, for SPI, the regions with a projected decrease of both drought variables (DF and DS) are clearly the majority; on the other hand, the net difference between regions with an increase and those with a decrease of both DF and DS is positive for SPEI.

One of the main consequences of climate change is that record-breaking (i.e., never previously recorded) extreme events are expected to happen, such as the 2010 Russian drought and heatwave (Trenberth and Fasullo 2012; Dosio et al. 2018). To estimate this possible evolution in the twenty-first century, we calculated how many events in 2071–2100 are projected to be more severe than the most severe ones that occurred in 1981–2010 (PK; Fig. 10). For SPI, under both scenarios, this will occur over approximately 33% of the unmasked lands. Moreover, for SPI under RCP8.5, only western South America, the Mediterranean region, and the Mediterranean-like southwestern parts of southern Africa will experience three or more droughts never recorded in 1981–2010 (see Table 5). For SPEI, such extreme droughts not recorded in 1981–2010 will involve approximately 75% of the unmasked lands under both scenarios and, under RCP8.5, 40% will face at least three such unrecorded events. According to Table 5, only a few regions will be hit by unrecorded events over less than

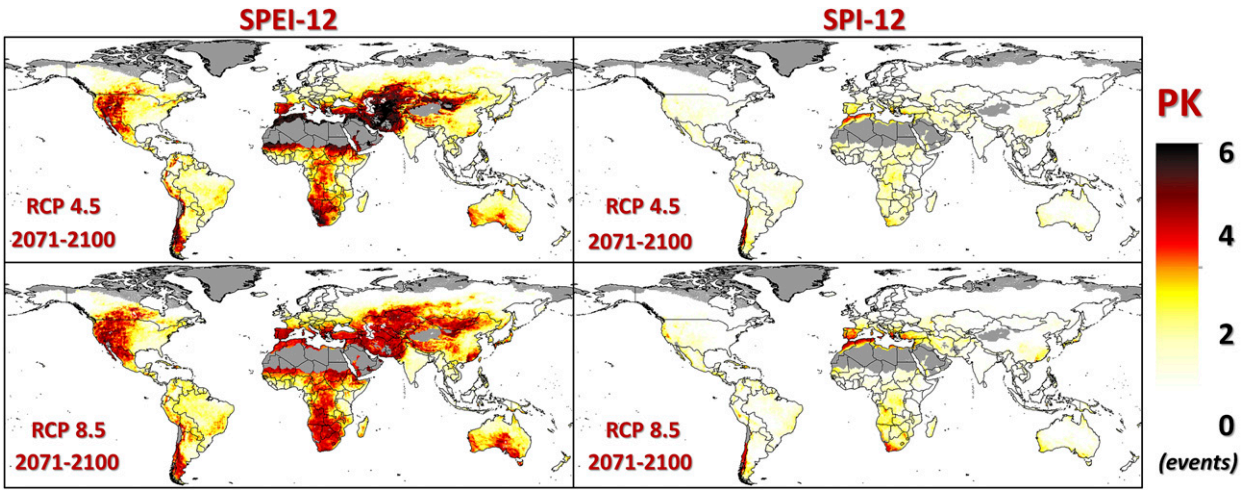

FIG. 10. Ensemble median number of drought events in 2071–2100 [(top) RCP4.5; (bottom) RCP8.5] being more severe than the most severe drought event that occurred in 1981–2010. Over areas with 0 peak events, no drought in 2071–2100 is projected to be more severe than the most severe in 1981–2010.

80% of their area, under both scenarios: high-latitude areas (Alaska, Canada–Greenland–Iceland, northern Europe, and northern Asia) and Southeast Asia.

d. The role of temperature in projections of meteorological drought

Comparisons of SPI and SPEI at global scale dealing with drought projections and based on GCMs are available in literature (e.g., Touma et al. 2015); in contrast, at the time of writing, no corresponding detailed study is available that uses RCM-based projections. Global drought projections based on SPI and SPEI are quite difficult to find, but some studies can serve for comparison with our new projections. For example, those based on SPI (Orlowsky and Seneviratne 2013) show a remarkable agreement in spatial patterns with our results. This indirectly confirms that meteorological drought projections based only on precipitation generally tend to agree, while more differences can be found at regional scale when temperature and evapotranspiration are considered (Cook et al. 2014; Touma et al. 2015; Dai et al. 2018), although it is important to highlight that the comparisons might depend on the different models used.

The most frequently used meteorological drought indicator including evapotranspiration is the Palmer drought severity index (PDSI) (Palmer 1965), which performs similarly to SPEI at medium to long accumulation periods (Beguería et al. 2014). The overall spatial patterns of drought projections computed using PDSI, both with older generation GCMs (Burke et al. 2006; Sheffield and Wood 2008) and more recent GCMs (Zhao and Dai 2015, 2017), agree with our results based on SPEI and CORDEX data. In particular, a very good correlation is found in areas characterized by an increase in drought variables such as southern South America (Penalba and Rivera 2013), the U.S. central plains and southwestern North America (Cook et al. 2015), the Mediterranean region (Diffenbaugh et al. 2007; Dubrovský et al. 2014), and southern Africa (Wang 2005; Zhao and Dai 2015, 2017). In other regions, such as the Amazon basin (Burke et al. 2006; Duffy et al. 2015), China (Wang and Chen 2014; L. Wang et al. 2014; Leng et al. 2015), and Australia (Kirono and Kent 2011), the projections are more uncertain (i.e., the changes are not robust in sign).

When evapotranspiration (and therefore temperature) is included, results are more complex to interpret. Recently, a few studies on drought projections dealing with the relative importance of evapotranspiration and rainfall at macroregional scale—that is, over North America (Jeong et al. 2014) and Europe (Spinoni et al. 2018)—have emerged. In both cases, over specific areas, the projected increase in evapotranspiration (drying tendency) is able to outweigh the projected increase in precipitation (wetting tendency), resulting in an increase in the values of the drought variables. Thus, drought projections based on precipitation only would result in opposite meteorological drought tendencies from those based on both precipitation and evapotranspiration. Here we investigate such divergent tendencies at a global scale based on the CORDEX RCM results.

Figure 11 shows where the SPEI and SPI agree or disagree on DF, DS, and peak events (PK) tendencies. The upper four panels help to determine the driver(s) of meteorological drought. DF and DS show similar spatial patterns for both scenarios over southern South America, the Mediterranean region, southern Africa,

TABLE 5. Percentage of area in which peak drought events (PK) that are more severe than the most severe drought in 1981–2010 are projected to occur at least once (≥1) or three or more times (≥3) during 2071–2100.

	RCP4.5				RCP8.5			
PK (area %)	SPI-12		SPEI-12		SPI-12		SPEI-12	
Region	≥1	≥3	≥1	≥3	≥1	≥3	≥1	≥3
ALA	0.0	0.0	13.9	0.0	0.0	0.0	7.9	0.0
CGI	1.0	0.0	29.6	5.6	0.4	0.0	29.0	13.4
WNA	30.6	0.0	90.7	57.6	40.8	0.9	90.2	71.7
CNA	17.2	0.0	92.5	12.7	17.6	0.0	97.1	30.4
ENA	4.2	0.0	83.8	6.6	1.5	0.0	95.6	3.8
CAM	53.5	0.4	96.7	29.0	68.0	2.5	92.4	37.7
AMZ	23.4	0.0	88.9	3.8	30.7	0.0	96.7	5.2
NEB	42.7	0.0	82.9	5.3	52.6	0.1	88.6	10.5
WSA	75.1	24.1	95.8	71.0	77.1	31.3	96.0	66.7
SSA	48.8	0.2	94.5	17.1	38.6	0.7	93.6	28.0
NEU	4.9	0.0	26.9	0.0	0.1	0.0	13.3	0.0
CEU	13.9	0.0	95.4	1.8	28.3	0.0	90.5	8.8
MED	98.8	14.7	100.0	89.7	99.7	47.1	100.0	96.1
WAF	65.6	0.1	96.3	46.0	55.2	0.9	97.5	59.3
EAF	42.3	0.0	91.4	37.1	37.8	0.3	93.1	47.6
SAF	93.9	1.1	99.7	68.4	94.5	10.5	100.0	82.7
NAS	0.6	0.0	51.5	9.5	0.9	0.0	51.3	20.7
WAS	73.4	0.0	100.0	97.1	72.3	0.5	100.0	98.2
CAS	46.3	0.0	100.0	93.7	40.4	0.0	100.0	97.3
TIB	2.1	0.0	100.0	72.5	2.0	0.0	100.0	82.3
EAS	27.1	0.0	97.5	20.6	28.7	0.7	99.2	47.6
SAS	12.6	0.0	67.9	17.5	9.9	0.0	81.4	20.5
SEA	25.5	0.2	52.8	1.3	24.9	0.3	57.5	2.5
NAU	27.8	0.1	91.9	16.9	23.9	0.1	98.0	27.4
SAU	45.8	0.0	92.2	33.8	59.9	2.5	95.4	60.3
GLOBE	32.7	0.8	74.7	32.8	32.7	2.5	76.2	40.0

southeastern China, and sparse areas in western North America and southern Australia. In these regions, both indicators project an increase in the drought variables, suggesting that droughts will become more frequent and severe due to a combination of both warming and drying. On the contrary, both indicators show a decrease over high latitudes in the Northern Hemisphere, Malaysia, and Indonesia, suggesting that the increase in precipitation (wetting) is projected to outweigh the increase in evapotranspiration (warming) in these regions. Over western Canada, central Europe, southern Siberia, eastern Africa, and India, the increase in precipitation counterbalances the increase in evapotranspiration, and thus the drought variables show a decrease only for SPI and no change for SPEI. Finally, over central and western North America, tropical Africa, the Middle East, and sparse areas over China and Australia—where no robust (in both sign and magnitude) change in precipitation is projected (see Fig. 4)—we note an increase in the frequency and severity of drought events only for SPEI, due to the effect of the increasing temperatures.

The green areas in the upper panels of Fig. 11 show contradicting drought tendencies: according to SPEI the drought variables are projected to increase, but according to SPI they are projected to decrease. Consequently, in these regions (mainly central Asia and Australia) the increase in precipitation will not be strong enough to outweigh the effect of increasing temperature (and, thus, the evapotranspiration), explaining why the drought variables increase for SPEI. These two regions will be characterized by a hot and wet future, potentially being exposed to even more weather extremes.

As shown in Fig. 4, temperature is projected to increase over the entire world. By combining this information with the upper panels in Fig. 11, we can highlight regions with the following characteristics:

- There is no leading driver; that is, both precipitation decrease and temperature increase will lead to an increase in drought frequency (red areas).
- Temperature increase is the leading driver for a drought frequency increase (pink areas).
- Precipitation and temperature increase are balanced, so only SPI projects a drought frequency decrease (light blue areas).
- Precipitation increase is the leading driver toward a drought frequency decrease (blue areas).
- Temperature increase is the leading driver: if taken into account, this leads to a drought frequency increase, if not, the precipitation increase leads to a drought frequency decrease (green areas).

The third row of panels in Fig. 11 shows the regions where extreme droughts unrecorded in the recent past are projected to occur in the future. By adding such information to those extracted from the first two rows of panels, we can answer the following question: where will the droughts be more frequent, severe, and extreme? This ''worst case'' is marked in dark red in the lower panels (ALL), where both the indicators show a robust (in sign) increase in all the three drought variables. We define such dark red areas as the future meteorological drought hot spots:

- The North American west coast, most of Mexico, northern Central America, and the Dominican Republic (RCP8.5).
- Chile and southwestern Argentina (both RCPs).
- The Mediterranean region (both RCPs).
- Parts of Congo (RCP4.5), Angola, Namibia, South Africa, and Madagascar (both RCPs).
- Southeastern China (both RCPs) and Japan (RCP8.5).
- Southwestern Australia and Tasmania (RCP8.5).

Conversely, over dark blue areas both indicators project less frequent and severe events and no unrecorded

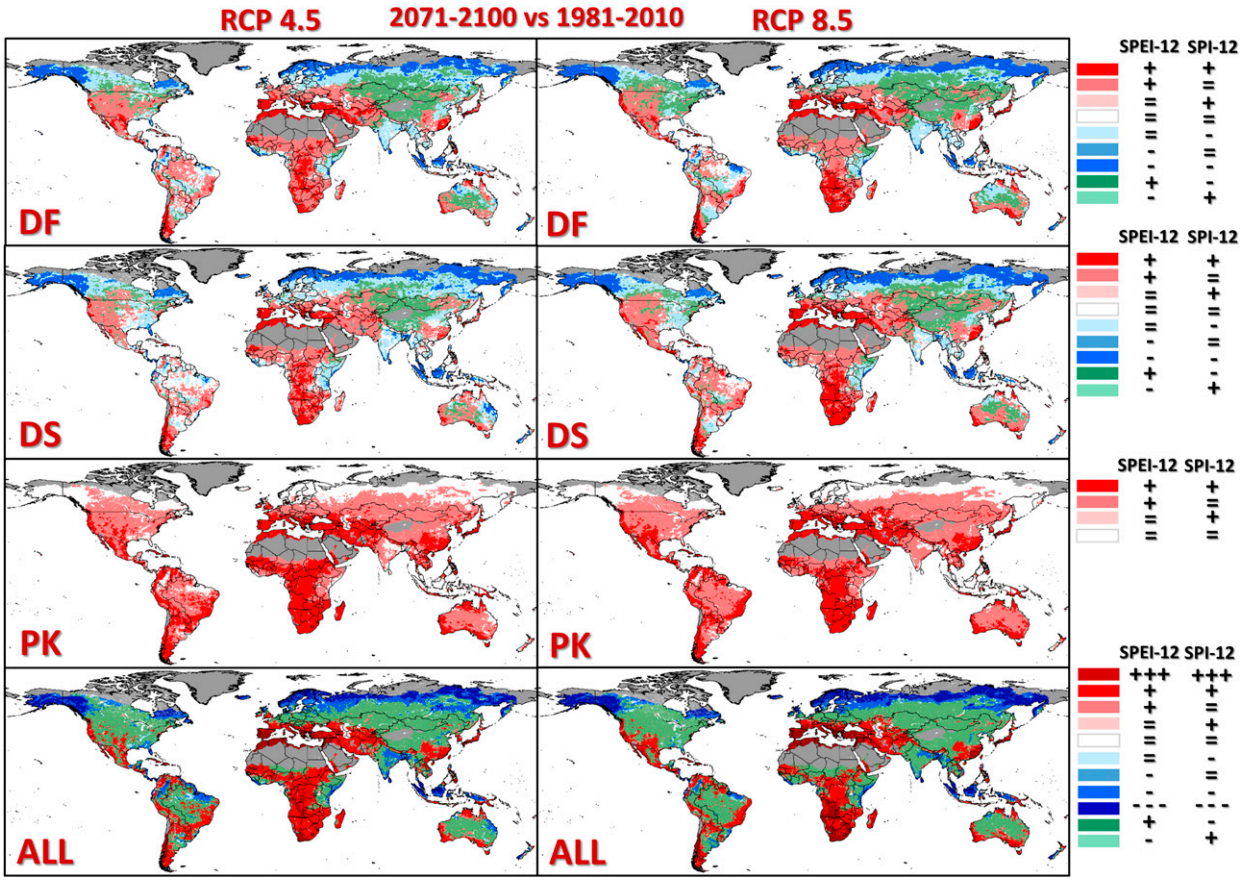

FIG. 11. Concordance between drought indicators (SPEI-12 and SPI-12) over the sign of change between 1981–2010 and 2071–2100. If the increase (+) or the decrease (−) is not robust (less than two-thirds of the simulations agree on sign), we use the symbol (=). Green areas represent contradicting tendencies. The bottom panels refer to the combined increase or decrease of the drought variables (DF, frequency; DS, severity; PK, peak events): the two extra categories (dark red and dark blue) represent an increase or decrease of all drought quantities for both indicators.

extreme droughts in the latter decades of the twenty-first century. Both climate scenarios agree on such areas: Alaska, northwestern and northeastern Canada, northern Scandinavia and Russia (including western Kamchatka), Sri Lanka, Malaysia, Indonesia, and southwestern New Zealand.

All of the above-mentioned regions—that is, the red (drought increase) and blue (drought decrease) areas—are characterized by robust and concordant projections by both indicators, but not always for all the three drought variables.

Finally, the green areas represent those regions where at least two drought variables out of three are projected to increase for SPEI and to decrease for SPI. Such areas are widespread over all continents, representing the largest category in North America, Asia, and Australia. There, the most frequent combination of projections is that where the drought events will be more frequent or more severe for SPEI, and less frequent or less severe for SPI. In addition, for SPEI, extreme events unrecorded in the past will appear in the future, but not for SPI. This combination is common over regions with mixed tendencies depending on the indicator selected, proving that the choice of the indicator is crucial, and that excluding temperature could lead to incomplete—or even misleading—results when dealing with meteorological drought projections.

4. Summary and conclusions

All of the simulations used in this study are in agreement regarding a progressive warming over the entire world. By the end of the twenty-first century, mean temperature is projected to increase between 2.6°C (under RCP4.5) and 4.8°C (RCP8.5) relative to 1981–2010. Such an increase is likely to lead to a remarkable increase in evaporative demand, which, when combined with a decrease in precipitation, may result in a shift

toward more arid climates. In this context, and considering that projected climate change is likely to result in more frequent and severe weather-related extremes (Sillmann et al. 2013; IPCC 2014), it is of the highest importance to investigate over which regions extreme events, such as meteorological droughts, are likely to become more frequent and/or severe, or even to lead to previously unrecorded extremes.

Our global analysis makes use of 103 climate simulations, based on a combination of GCMs and RCMs, derived from the CORDEX experiment. This study has two main headline features:

- This is the first global attempt to analyze drought projections using RCMs with a spatial resolution of 0.44°, which at the time of writing is the highest available (higher-resolution data are available only for very few domains).
- The separate use of the SPEI and SPI indicators allows an in-depth investigation of the critical role of temperature when dealing with meteorological droughts, something that was discussed in studies based on GCMs (Touma et al. 2015), but never at global scale using RCMs as input.

We investigated changes in drought frequency and severity, and the occurrence of extreme events between the periods 1981–2010 and 2071–2100. Over 1981–2010, we also performed a validation versus observational datasets. Results show that the areas where these drought variables are projected to increase are larger if SPEI (which indirectly includes temperature) is used instead of SPI (which considers precipitation only). However, both indicators agree on projecting fewer and less severe drought events over high latitudes in the Northern Hemisphere and over southeastern Asia [where seasonal projections may show different tendencies, as discussed by Tangang et al. (2018)]. Conversely, they agree on more frequent and severe drought events, especially under the RCP8.5 climate scenario, over southern South America, the Mediterranean region, southern Africa, southeastern China, Japan, and southern Australia.

As previously done for single regions (e.g., by Tabari and Willems 2018), we compared the results obtained by using the CORDEX simulations versus those obtained by using the parent GCMs only. The improvement in the spatial resolution (from 1.8° to 0.44°) is not the only benefit introduced by the RCMs. Overall, the spatial patterns in drought changes projected by CORDEX and GCMs are similar, but, depending on the climate scenario and the indicator, we found some discrepancies, in particular over the western United States, South America, tropical Africa, and central Australia. This supports the opinion that the use of RCMs in climate projections adds critical information also at global scale.

Over some regions, the meteorological drought tendency for the end of the twenty-first century crucially depends on the choice of the indicator, in other words on the inclusion or exclusion of temperature (and evapotranspiration) as a climate driver. This occurs in particular over North America, Amazonia, central Europe, central Asia, the Horn of Africa, and central Australia. One of the consequences of this is that the choice of indicator can be crucial in assessment of the impact of droughts for different socioeconomic sectors and/or ecosystems, depending on the importance of evapotranspiration. For example, agriculture can be severely affected by meteorological droughts, because crops are sensitive to evapotranspiration (Jensen and Allen 2016), while river transportation can be less impacted, because the level of rivers mainly depends on precipitation (Peterson et al. 2008).

Meteorological droughts will likely increase in frequency and severity in large areas of the world. Many of these regions are already now suffering from water scarcity (Cherlet et al. 2018). Key drivers here are a decrease in rainfall, or an increased evaporative demand due to increasing temperatures, or a combination of both. A better understanding of these projections requires an analysis of how these meteorological conditions translate into soil moisture and hydrological droughts and their relation with impacts on societies and the environment.

The presented maps, tables, and gridded outputs used in this study will be made available and freely accessible through the European Commission's Global Drought Observatory (GDO) online platform. It is planned to build on the results of this study in order to combine drought hazard projections with projections of factors of exposure and vulnerability under different socioeconomic scenarios (van Vuuren et al. 2014), for assessing future drought risk—similarly to what has been done for the past decades by Carrão et al. (2016).

Acknowledgments. We acknowledge the World Climate Research Programme's Working Group on Regional Climate, and the Working Group on Coupled Modelling, former coordinating body of CORDEX and responsible panel for CMIP5. We also thank Erik van Meijgaard, Klaus Keuler, J. Sanjay, Jerasorn Santisirisomboon, Samuel Somot, Wenxin Zhang, and all the climate modelling groups that produced and made available their model output. We also acknowledge the Earth System Grid Federation infrastructure, an international

effort led by the U.S. Department of Energy's Program for Climate Model Diagnosis and Intercomparison, the European Network for Earth System Modelling, and other partners in the Global Organisation for Earth System Science Portals (GO-ESSP).

REFERENCES

Ackerley, D., and D. Dommenget, 2016: Atmosphere-only GCM (ACCESS1.0) simulations with prescribed land surface temperatures. *Geosci. Model Dev.*, **9**, 2077–2098, https://doi.org/10.5194/gmd-9-2077-2016.

Allen, R. G., and Coauthors, 2006: A recommendation on standardized surface resistance for hourly calculation of reference ET_o by the FAO56 Penman-Monteith method. *Agric. Water Manage.*, **81**, 1–22, https://doi.org/10.1016/j.agwat.2005.03.007.

Bai, Z. G., D. L. Dent, L. Olsson, and M. E. Schaepman, 2008: Proxy global assessment of land degradation. *Soil Use Manage.*, **24**, 223–234, https://doi.org/10.1111/j.1475-2743.2008.00169.x.

Bartos, M. D., and M. V. Chester, 2015: Impacts of climate change on electric power supply in the western United States. *Nat. Climate Change*, **5**, 748–752, https://doi.org/10.1038/nclimate2648.

Becker, A., P. Finger, A. Meyer-Christoffer, B. Rudolf, K. Schamm, U. Schneider, and M. Ziese, 2013: A description of the global land-surface precipitation data products of the Global Precipitation Climatology Centre with sample applications including centennial (trend) analysis from 1901–present. *Earth Syst. Sci. Data*, **5**, 71–99, https://doi.org/10.5194/essd-5-71-2013.

Beguería, S., S. M. Vicente-Serrano, F. Reig, and B. Latorre, 2014: Standardized Precipitation Evapotranspiration Index (SPEI) revisited: Parameter fitting, evapotranspiration models, tools, datasets and drought monitoring. *Int. J. Climatol.*, **34**, 3001–3023, https://doi.org/10.1002/joc.3887.

Bentsen, M., and Coauthors, 2013: The Norwegian Earth System Model, NorESM1-M—Part 1: Description and basic evaluation of the physical climate. *Geosci. Model Dev.*, **6**, 687–720, https://doi.org/10.5194/gmd-6-687-2013.

Bi, D., and Coauthors, 2013: The ACCESS coupled model: Description, control climate and evaluation. *Aust. Meteor. Oceanogr. J.*, **63**, 41–64, https://doi.org/10.22499/2.6301.004.

Brutsaert, W., and M. B. Parlange, 1998: Hydrologic cycle explains the evaporation paradox. *Nature*, **396**, 30, https://doi.org/10.1038/23845.

Burke, E. J., and S. J. Brown, 2008: Evaluating uncertainties in the projection of future drought. *J. Hydrometeor.*, **9**, 292–299, https://doi.org/10.1175/2007JHM929.1.

——, ——, and N. Christidis, 2006: Modeling the recent evolution of global drought and projections for the twenty-first century with the Hadley Centre climate model. *J. Hydrometeor.*, **7**, 1113–1125, https://doi.org/10.1175/JHM544.1.

Carrão, H., G. Naumann, and P. Barbosa, 2016: Mapping global patterns of drought risk: An empirical framework based on sub-national estimates of hazard, exposure and vulnerability. *Global Environ. Change*, **39**, 108–124, https://doi.org/10.1016/j.gloenvcha.2016.04.012.

Cherlet, M., C. Hutchinson, J. Reynolds, J. Hill, S. Sommer, and G. von Matitz, Eds., 2018: *World Atlas of Desertification: Rethinking Land Degradation and Sustainable Land Management*. 3rd ed. Publication Office of the European Union, 248 pp.

Christensen, O. B., M. Drews, J. H. Christensen, K. Dethloff, K. Ketelsen, I. Hebestadt, and A. Rinke, 2006: The HIRHAM regional climate model version 5 (β). DMI Tech. Rep. 06–17, 22 pp., https://www.dmi.dk/fileadmin/Rapporter/TR/tr06-17.pdf.

Chylek, P., J. Li, M. K. Dubey, M. Wang, and G. Lesins, 2011: Observed and model simulated 20th century Arctic temperature variability: Canadian Earth System Model CanESM2. *Atmos. Chem. Phys. Discuss.*, **11**, 22 893–22 907, https://doi.org/10.5194/acpd-11-22893-2011.

Coelho, C. A., and Coauthors, 2016: The 2014 southeast Brazil austral summer drought: Regional scale mechanisms and teleconnections. *Climate Dyn.*, **46**, 3737–3752, https://doi.org/10.1007/s00382-015-2800-1.

Collins, W. J., and Coauthors, 2011: Development and evaluation of an Earth-system model–HadGEM2. *Geosci. Model Dev.*, **4**, 1051–1075, https://doi.org/10.5194/gmd-4-1051-2011.

Colorado-Ruiz, G., T. Cavazos, J. A. Salinas, P. De Grau, and R. Ayala, 2018: Climate change projections from Coupled Model Intercomparison Project phase 5 multi-model weighted ensembles for Mexico, the North American monsoon, and the mid-summer drought region. *Int. J. Climatol.*, **38**, 5699–5716, https://doi.org/10.1002/joc.5773.

Cook, B. I., J. E. Smerdon, R. Seager, and S. Coats, 2014: Global warming and 21st century drying. *Climate Dyn.*, **43**, 2607–2627, https://doi.org/10.1007/s00382-014-2075-y.

——, T. R. Ault, and J. E. Smerdon, 2015: Unprecedented 21st century drought risk in the American Southwest and Central Plains. *Sci. Adv.*, **1**, e1400082, https://doi.org/10.1126/sciadv.1400082.

——, K. J. Anchukaitis, R. Touchan, D. M. Meko, and E. R. Cook, 2016: Spatiotemporal drought variability in the Mediterranean over the last 900 years. *J. Geophys. Res. Atmos.*, **121**, 2060–2074, https://doi.org/10.1002/2015JD023929.

Crausbay, S. D., and Coauthors, 2017: Defining ecological drought for the twenty-first century. *Bull. Amer. Meteor. Soc.*, **98**, 2543–2550, https://doi.org/10.1175/BAMS-D-16-0292.1.

Cressie, N., 1990: The origins of kriging. *Math. Geol.*, **22**, 239–252, https://doi.org/10.1007/BF00889887.

Dai, A., 2011: Drought under global warming: A review. *Wiley Interdiscip. Rev.: Climate Change*, **2**, 45–65, https://doi.org/10.1002/WCC.81.

——, 2013: Increasing drought under global warming in observations and models. *Nat. Climate Change*, **3**, 52–58, https://doi.org/10.1038/nclimate1633.

——, and T. Zhao, 2017: Uncertainties in historical changes and future projections of drought. Part I: Estimates of historical drought changes. *Climatic Change*, **144**, 519–533, https://doi.org/10.1007/s10584-016-1705-2.

——, ——, and J. Chen, 2018: Climate change and drought: A precipitation and evaporation perspective. *Curr. Climate Change Rep.*, **4**, 301–312, https://doi.org/10.1007/S40641-018-0101-6.

Diasso, U., and B. J. Abiodun, 2017: Drought modes in West Africa and how well CORDEX RCMs simulate them. *Theor. Appl. Climatol.*, **128**, 223–240, https://doi.org/10.1007/s00704-015-1705-6.

Diffenbaugh, N. S., J. S. Pal, F. Giorgi, and X. Gao, 2007: Heat stress intensification in the Mediterranean climate change hotspot. *Geophys. Res. Lett.*, **34**, L11706, https://doi.org/10.1029/2007GL030000.

Di Luca, A., R. de Elía, and R. Laprise, 2012: Potential for added value in precipitation simulated by high-resolution nested regional climate models and observations. *Climate Dyn.*, **38**, 1229–1247, https://doi.org/10.1007/s00382-011-1068-3.

Diro, G. T., L. Sushama, A. Martynov, D. I. Jeong, D. Verseghy, and K. Winger, 2014: Land–atmosphere coupling over North America in CRCM5. *J. Geophys. Res. Atmos.*, **119**, 11 955–11 972, https://doi.org/10.1002/2014JD021677.

Donner, L. J., and Coauthors, 2011: The dynamical core, physical parameterizations, and basic simulation characteristics of the atmospheric component AM3 of the GFDL global coupled model CM3. *J. Climate*, **24**, 3484–3519, https://doi.org/10.1175/2011JCLI3955.1.

Dosio, A., 2017: Projection of temperature and heat waves for Africa with an ensemble of CORDEX regional climate models. *Climate Dyn.*, **49**, 493–519, https://doi.org/10.1007/s00382-016-3355-5.

——, H. J. Panitz, M. Schubert-Frisius, and D. Lüthi, 2015: Dynamical downscaling of CMIP5 global circulation models over CORDEX-Africa with COSMO-CLM: Evaluation over the present climate and analysis of the added value. *Climate Dyn.*, **44**, 2637–2661, https://doi.org/10.1007/s00382-014-2262-x.

——, L. Mentaschi, E. M. Fischer, and K. Wyser, 2018: Extreme heat waves under 1.5°C and 2°C global warming. *Environ. Res. Lett.*, **13**, 054006, https://doi.org/10.1088/1748-9326/aab827.

——, R. G. Jones, C. Jack, C. Lennard, G. Nikulin, and B. Hewitson, 2019: What can we know about future precipitation in Africa? Robustness, significance and added value of projections from a large ensemble of regional climate models. *Climate Dyn.*, **53**, 5833–5858, https://doi.org/10.1007/s00382-019-04900-3.

Dubrovský, M., M. Hayes, P. Duce, M. Trnka, M. Svoboda, and P. Zara, 2014: Multi-GCM projections of future drought and climate variability indicators for the Mediterranean region. *Reg. Environ. Change*, **14**, 1907–1919, https://doi.org/10.1007/s10113-013-0562-z.

Duffy, P. B., P. Brando, G. P. Asner, and C. B. Field, 2015: Projections of future meteorological drought and wet periods in the Amazon. *Proc. Natl. Acad. Sci. USA*, **112**, 13 172–13 177, https://doi.org/10.1073/pnas.1421010112.

Dufresne, J. L., and Coauthors, 2013: Climate change projections using the IPSL-CM5 Earth system model: From CMIP3 to CMIP5. *Climate Dyn.*, **40**, 2123–2165, https://doi.org/10.1007/s00382-012-1636-1.

Dunne, J. P., and Coauthors, 2012: GFDL's ESM2 global coupled climate–carbon Earth system models. Part I: Physical formulation and baseline simulation characteristics. *J. Climate*, **25**, 6646–6665, https://doi.org/10.1175/JCLI-D-11-00560.1.

——, and Coauthors, 2013: GFDL's ESM2 global coupled climate–carbon Earth system models. Part II: Carbon system formulation and baseline simulation characteristics. *J. Climate*, **26**, 2247–2267, https://doi.org/10.1175/JCLI-D-12-00150.1.

Feser, F., B. Rockel, H. von Storch, J. Winterfeldt, and M. Zahn, 2011: Regional climate models add value to global model data: A review and selected examples. *Bull. Amer. Meteor. Soc.*, **92**, 1181–1192, https://doi.org/10.1175/2011BAMS3061.1.

Gent, P. R., and Coauthors, 2011: The Community Climate System Model version 4. *J. Climate*, **24**, 4973–4991, https://doi.org/10.1175/2011JCLI4083.1.

Giorgetta, M. A., and Coauthors, 2013: Climate and carbon cycle changes from 1850 to 2100 in MPI-ESM simulations for the Coupled Model Intercomparison Project phase 5. *J. Adv. Model. Earth Syst.*, **5**, 572–597, https://doi.org/10.1002/jame.20038.

Giorgi, F., and J. Gutowski Jr., 2015: Regional dynamical downscaling and the CORDEX initiative. *Annu. Rev. Environ. Resour.*, **40**, 467–490, https://doi.org/10.1146/annurev-environ-102014-021217.

——, C. Jones, and G. R. Asrar, 2009: Addressing climate information needs at the regional level: The CORDEX framework. *WMO Bull.*, **58**, 175–183, https://public.wmo.int/en/bulletin/addressing-climate-information-needs-regional-level-cordex-framework.

——, and Coauthors, 2014: Changes in extremes and hydroclimatic regimes in the CREMA ensemble projections. *Climatic Change*, **125**, 39–51, https://doi.org/10.1007/s10584-014-1117-0.

Hanel, M., O. Rakovec, Y. Markonis, P. Máca, L. Samaniego, J. Kyselý, and R. Kumar, 2018: Revisiting the recent European droughts from a long-term perspective. *Sci. Rep.*, **8**, 9499, https://doi.org/10.1038/s41598-018-27464-4.

Hargreaves, G. H., and Z. A. Samani, 1985: Reference crop evapotranspiration from temperature. *Appl. Eng. Agric.*, **1**, 96–99, https://doi.org/10.13031/2013.26773.

Harris, I., P. D. Jones, T. J. Osborn, and D. H. Lister, 2014: Updated high-resolution grids of monthly climatic observations—The CRU TS3. 10 dataset. *Int. J. Climatol.*, **34**, 623–642, https://doi.org/10.1002/joc.3711.

Hauser, M., and Coauthors, 2017: Methods and model dependency of extreme event attribution: The 2015 European drought. *Earth's Future*, **5**, 1034–1043, https://doi.org/10.1002/2017EF000612.

Hazeleger, W., and Coauthors, 2010: EC-Earth: A seamless Earth system prediction approach in action. *Bull. Amer. Meteor. Soc.*, **91**, 1357–1364, https://doi.org/10.1175/2010BAMS2877.1.

Heim, R. R., Jr., 2002: A review of twentieth-century drought indices used in the United States. *Bull. Amer. Meteor. Soc.*, **83**, 1149–1166, https://doi.org/10.1175/1520-0477-83.8.1149.

Hewitson, B. C., and R. G. Crane, 1996: Climate downscaling: Techniques and application. *Climate Res.*, **7**, 85–95, https://doi.org/10.3354/cr007085.

Hewitt, H. T., D. Copsey, I. D. Culverwell, C. M. Harris, R. S. R. Hill, A. B. Keen, A. J. McLaren, and E. C. Hunke, 2011: Design and implementation of the infrastructure of HadGEM3: The next-generation Met Office climate modelling system. *Geosci. Model Dev.*, **4**, 223–253, https://doi.org/10.5194/gmd-4-223-2011.

Hosseinzadehtalaei, P., H. Tabari, and P. Willems, 2017: Quantification of uncertainty in reference evapotranspiration climate change signals in Belgium. *Hydrol. Res.*, **48**, 1391–1401, https://doi.org/10.2166/nh.2016.243.

Iglesias, A., L. Garrote, A. Cancelliere, F. Cubillo, and D. A. Wilhite, Eds., 2009: *Coping with Drought Risk in Agriculture and Water Supply Systems: Drought Management and Policy Development in the Mediterranean*. Springer, 320 pp.

IPCC, 2012: *Managing the Risks of Extreme Events and Disasters to Advance Climate Change Adaptation.* C. B. Field et al., Eds., Cambridge University Press, 582 pp., https://www.ipcc.ch/site/assets/uploads/2018/03/SREX_Full_Report-1.pdf.

——, 2014: *Climate Change 2014: Synthesis Report.* R. K. Pachauri and L. A. Meyer, Eds., IPCC, 151 pp., https://www.ipcc.ch/site/assets/uploads/2018/02/SYR_AR5_FINAL_full.pdf.

Jacob, D., and Coauthors, 2012: Assessing the transferability of the regional climate model REMO to different Coordinated Regional Climate Downscaling Experiment (CORDEX) regions. *Atmosphere*, **3**, 181–199, https://doi.org/10.3390/atmos3010181.

Jeffrey, S. J., L. D. Rotstayn, M. A. Collier, S. Dravitzki, C. Hamalainen, C. Moeseneder, K. K. Wong, and J. Syktus, 2013: Australia's CMIP5 submission using the CSIRO Mk3.6

model. *Aust. Meteor. Oceanogr. J.*, **63**, 1–13, https://doi.org/10.22499/2.6301.001.

Jensen, M. E., and R. G. Allen, Eds., 2016: *Evaporation, Evapotranspiration, and Irrigation Water Requirements*. American Society of Civil Engineers, 744 pp.

Jeong, D. I., L. Sushama, and M. N. Khaliq, 2014: The role of temperature in drought projections over North America. *Climatic Change*, **127**, 289–303, https://doi.org/10.1007/s10584-014-1248-3.

Kelley, C. P., S. Mohtadi, M. A. Cane, R. Seager, and Y. Kushnir, 2015: Climate change in the Fertile Crescent and implications of the recent Syrian drought. *Proc. Natl. Acad. Sci. USA*, **112**, 3241–3246, https://doi.org/10.1073/pnas.1421533112.

Kendon, E. J., and Coauthors, 2017: Do convection-permitting regional climate models improve projections of future precipitation change? *Bull. Amer. Meteor. Soc.*, **98**, 79–93, https://doi.org/10.1175/BAMS-D-15-0004.1.

Kirono, D. G., and D. M. Kent, 2011: Assessment of rainfall and potential evaporation from global climate models and its implications for Australian regional drought projection. *Int. J. Climatol.*, **31**, 1295–1308, https://doi.org/10.1002/joc.2165.

Knutti, R., and J. Sedláček, 2013: Robustness and uncertainties in the new CMIP5 climate model projections. *Nat. Climate Change*, **3**, 369–373, https://doi.org/10.1038/nclimate1716.

——, ——, B. M. Sanderson, R. Lorenz, E. M. Fischer, and V. Eyring, 2017: A climate model projection weighting scheme accounting for performance and interdependence. *Geophys. Res. Lett.*, **44**, 1909–1918, https://doi.org/10.1002/2016GL072012.

Koenigk, T., L. Brodeau, R. G. Graversen, J. Karlsson, G. Svensson, M. Tjernström, U. Willén, and K. Wyser, 2013: Arctic climate change in 21st century CMIP5 simulations with EC-Earth. *Climate Dyn.*, **40**, 2719–2743, https://doi.org/10.1007/s00382-012-1505-y.

Leng, G., Q. Tang, and S. Rayburg, 2015: Climate change impacts on meteorological, agricultural and hydrological droughts in China. *Global Planet. Change*, **126**, 23–34, https://doi.org/10.1016/j.gloplacha.2015.01.003.

Li, Y., W. Ye, M. Wang, and X. Yan, 2009: Climate change and drought: A risk assessment of crop-yield impacts. *Climate Res.*, **39**, 31–46, https://doi.org/10.3354/cr00797.

Llopart, M., E. Coppola, F. Giorgi, R. P. Da Rocha, and S. V. Cuadra, 2014: Climate change impact on precipitation for the Amazon and La Plata basins. *Climatic Change*, **125**, 111–125, https://doi.org/10.1007/s10584-014-1140-1.

Lu, J., G. J. Carbone, and J. M. Grego, 2019: Uncertainty and hotspots in 21st century projections of agricultural drought from CMIP5 models. *Sci. Rep.*, **9**, 4922, https://doi.org/10.1038/s41598-019-41196-z.

Lucas-Picher, P., S. Somot, M. Déqué, B. Decharme, and A. Alias, 2013: Evaluation of the regional climate model ALADIN to simulate the climate over North America in the CORDEX framework. *Climate Dyn.*, **41**, 1117–1137, https://doi.org/10.1007/s00382-012-1613-8.

Madsen, M. S., P. L. Langen, F. Boberg, and J. H. Christensen, 2017: Inflated uncertainty in multimodel-based regional climate projections. *Geophys. Res. Lett.*, **44**, 11 606–11 613, https://doi.org/10.1002/2017GL075627.

Masante, D., N. McCormick, J. Vogt, C. Carmona-Moreno, E. Cordano, and I. Ameztoy, 2018: 2018—Drought and water crisis in Southern Africa. JRC Tech. Rep. 111596, 28 pp., https://publications.jrc.ec.europa.eu/repository/handle/JRC111596.

McGregor, J. L., and M. R. Dix, 2008: An updated description of the conformal-cubic atmospheric model. *High Resolution Numerical Modelling of the Atmosphere and Ocean*, K. Hamilton and W. Ohfuchi, Eds., Springer, 51–75.

McKee, T. B., N. J. Doesken, and J. Kleist, 1993: The relationship of drought frequency and duration to time scales. *Proc. Eighth Conf. on Applied Climatology*, Anaheim, CA, Amer. Meteor. Soc., 179–183.

McKenney, M. S., and N. J. Rosenberg, 1993: Sensitivity of some potential evapotranspiration estimation methods to climate change. *Agric. For. Meteor.*, **64**, 81–110, https://doi.org/10.1016/0168-1923(93)90095-Y.

Meehl, G. A., and Coauthors, 2007: Global climate projections. *Climate Change 2007: The Physical Science Basis*, S. Solomon et al., Eds., Cambridge University Press, 747–846.

——, and Coauthors, 2013: Climate change projections in CESM1(CAM5) compared to CCSM4. *J. Climate*, **26**, 6287–6308, https://doi.org/10.1175/JCLI-D-12-00572.1.

Menut, L., O. P. Tripathi, A. Colette, R. Vautard, E. Flaounas, and B. Bessagnet, 2012: Evaluation of regional climate simulations for air quality modeling purposes. *Climate Dyn.*, **40**, 2515–2533, https://doi.org/10.1007/s00382-012-1345-9.

Meresa, H. K., M. Osuch, and R. Romanowicz, 2016: Hydro-meteorological drought projections into the 21st century for selected Polish catchments. *Water*, **8**, 206, https://doi.org/10.3390/w8050206.

Milly, P. C., and K. A. Dunne, 2016: Potential evapotranspiration and continental drying. *Nat. Climate Change*, **6**, 946–949, https://doi.org/10.1038/nclimate3046.

Mishra, A. K., and V. P. Singh, 2010: A review of drought concepts. *J. Hydrol.*, **391**, 202–216, https://doi.org/10.1016/j.jhydrol.2010.07.012.

——, and ——, 2011: Drought modeling—A review. *J. Hydrol.*, **403**, 157–175, https://doi.org/10.1016/j.jhydrol.2011.03.049.

Naumann, G., J. Spinoni, J. V. Vogt, and P. Barbosa, 2015: Assessment of drought damages and their uncertainties in Europe. *Environ. Res. Lett.*, **10**, 124013, https://doi.org/10.1088/1748-9326/10/12/124013.

Orlowsky, B., and S. I. Seneviratne, 2012: Global changes in extreme events: Regional and seasonal dimension. *Climatic Change*, **110**, 669–696, https://doi.org/10.1007/s10584-011-0122-9.

——, and ——, 2013: Elusive drought: Uncertainty in observed trends and short- and long-term CMIP5 projections. *Hydrol. Earth Syst. Sci.*, **17**, 1765–1781, https://doi.org/10.5194/hess-17-1765-2013.

Osborn, T., J. Barichivich, I. Harris, G. van der Schrier, and P. Jones, 2016: Monitoring global drought using the self-calibrating Palmer drought severity index [in "State of the Climate in 2015"]. *Bull. Amer. Meteor. Soc.*, **97**, S32–S36, https://www.ametsoc.net/sotc/StateoftheClimate2015_lowres.pdf.

Ozturk, T., M. T. Turp, M. Türkeş, and M. L. Kurnaz, 2017: Projected changes in temperature and precipitation climatology of Central Asia CORDEX Region 8 by using RegCM4.3.5. *Atmos. Res.*, **183**, 296–307, https://doi.org/10.1016/j.atmosres.2016.09.008.

Palmer, W. C., 1965: Meteorological drought. U.S. Weather Bureau Research Paper 45, 58 pp., http://www.ncdc.noaa.gov/temp-and-precip/drought/docs/palmer.pdf.

Penalba, O. C., and J. A. Rivera, 2013: Future changes in drought characteristics over southern South America projected by a CMIP5 multi-model ensemble. *Amer. J. Climate Change*, **2**, 173–182, https://doi.org/10.4236/AJCC.2013.23017.

Peterson, T. C., M. McGuirk, T. G. Houston, A. H. Horvitz, and M. F. Wehner, 2008: Climate variability and change with implications for transportation. *20th Conf. on Climate Variability and Climate Change*, Washington, DC, Amer. Meteor. Soc., 4B.5, https://ams.confex.com/ams/pdfpapers/131039.pdf.

Power, S. B., F. Delage, R. Colman, and A. Moise, 2012: Consensus on twenty-first-century rainfall projections in climate models more widespread than previously thought. *J. Climate*, **25**, 3792–3809, https://doi.org/10.1175/JCLI-D-11-00354.1.

Prudhomme, C., and Coauthors, 2014: Hydrological droughts in the 21st century, hotspots and uncertainties from a global multimodel ensemble experiment. *Proc. Natl. Acad. Sci. USA*, **111**, 3262–3267, https://doi.org/10.1073/pnas.1222473110.

Reliefweb, 2019: Kenya: Drought—2014–2019. Accessed 30 June 2019, https://reliefweb.int/disaster/dr-2014-000131-ken.

Rockel, B., A. Will, and A. Hense, 2008: The regional climate model COSMO-CLM (CCLM). *Meteor. Z.*, **17**, 347–348, https://doi.org/10.1127/0941-2948/2008/0309.

Roderick, M. L., P. Greve, and G. D. Farquhar, 2015: On the assessment of aridity with changes in atmospheric CO_2. *Water Resour. Res.*, **51**, 5450–5463, https://doi.org/10.1002/2015WR017031.

Rummukainen, M., 2010: State-of-the-art with regional climate models. *Wiley Interdiscip. Rev.: Climate Change*, **1**, 82–96, https://doi.org/10.1002/WCC.8.

Samuelsson, P., S. Gollvik, C. Jansson, M. Kupiainen, E. Kourzeneva, and W. J. van de Berg, 2015: The surface processes of the Rossby Centre regional atmospheric climate model (RCA4). SMHI Rep. 157, 58 pp., http://www.smhi.se/polopoly_fs/1.89799!/Menu/gen.

Sánchez, E., and Coauthors, 2015: Regional climate modelling in CLARIS-LPB: A concerted approach towards twenty-first century projections of regional temperature and precipitation over South America. *Climate Dyn.*, **45**, 2193–2212, https://doi.org/10.1007/s00382-014-2466-0.

Schmidhuber, J., and F. N. Tubiello, 2007: Global food security under climate change. *Proc. Natl. Acad. Sci. USA*, **104**, 19 703–19 708, https://doi.org/10.1073/pnas.0701976104.

Schneider, U., T. Fuchs, A. Meyer-Christoffer, and B. Rudolf, 2008: Global precipitation analysis products of the GPCC. Global Precipitation Climatology Centre (GPCC), DWD, 112 pp.

Scinocca, J. F., and Coauthors, 2016: Coordinated global and regional climate modeling. *J. Climate*, **29**, 17–35, https://doi.org/10.1175/JCLI-D-15-0161.1.

Scoccimarro, E., and Coauthors, 2011: Effects of tropical cyclones on ocean heat transport in a high-resolution coupled general circulation model. *J. Climate*, **24**, 4368–4384, https://doi.org/10.1175/2011JCLI4104.1.

Seager, R., and Coauthors, 2007: Model projections of an imminent transition to a more arid climate in southwestern North America. *Science*, **316**, 1181–1184, https://doi.org/10.1126/SCIENCE.1139601.

Seneviratne, S. I., 2012: Historical drought trends revisited. *Nature*, **491**, 338–339, https://doi.org/10.1038/491338a.

Šeparović, L., A. Alexandru, R. Laprise, A. Martynov, L. Sushama, K. Winger, K. Tete, and M. Valin, 2013: Present climate and climate change over North America as simulated by the fifth-generation Canadian regional climate model. *Climate Dyn.*, **41**, 3167–3201, https://doi.org/10.1007/s00382-013-1737-5.

Shahidian, S., R. Serralheiro, J. Serrano, J. Teixeira, N. Haie, and F. Santos, 2012: Hargreaves and other reduced-set methods for calculating evapotranspiration. *Evapotranspiration: Remote Sensing and Modeling*, A. Irmark, Ed., IntechOpen, 59–80.

Sheffield, J., and E. F. Wood, 2008: Projected changes in drought occurrence under future global warming from multi-model, multi-scenario, IPCC AR4 simulations. *Climate Dyn.*, **31**, 79–105, https://doi.org/10.1007/s00382-007-0340-z.

——, ——, and M. L. Roderick, 2012: Little change in global drought over the past 60 years. *Nature*, **491**, 435–438, https://doi.org/10.1038/nature11575.

Sillmann, J., V. V. Kharin, F. W. Zwiers, X. Zhang, and D. Bronaugh, 2013: Climate extremes indices in the CMIP5 multimodel ensemble: Part 2. Future climate projections. *J. Geophys. Res. Atmos.*, **118**, 2473–2493, https://doi.org/10.1002/JGRD.50188.

Smiatek, G., J. Helmert, and E. M. Gerstner, 2016: Impact of land use and soil data specifications on COSMO-CLM simulations in the CORDEX-MED area. *Meteor. Z.*, **25**, 215–230, https://doi.org/10.1127/metz/2015/0594.

Spinoni, J., G. Naumann, H. Carrão, P. Barbosa, and J. Vogt, 2014: World drought frequency, duration, and severity for 1951–2010. *Int. J. Climatol.*, **34**, 2792–2804, https://doi.org/10.1002/joc.3875.

——, ——, J. Vogt, and P. Barbosa, 2015a: European drought climatologies and trends based on a multi-indicator approach. *Global Planet. Change*, **127**, 50–57, https://doi.org/10.1016/j.gloplacha.2015.01.012.

——, ——, and ——, 2015b: Spatial patterns of European droughts under a moderate emission scenario. *Adv. Sci. Res.*, **12**, 179–186, https://doi.org/10.5194/asr-12-179-2015.

——, J. V. Vogt, G. Naumann, P. Barbosa, and A. Dosio, 2018: Will drought events become more frequent and severe in Europe? *Int. J. Climatol.*, **38**, 1718–1736, https://doi.org/10.1002/joc.5291.

Spiridonov, V., M. Déqué, and S. Somot, 2005: ALADIN-Climate: From the origins to present date. *ALADIN Newsletter*, No. 29, 89–92.

Stahle, D. W., and Coauthors, 2009: Early 21st-century drought in Mexico. *Eos Trans. Amer. Geophys. Union*, **90**, 89–100, https://doi.org/10.1029/2009EO110001.

Strandberg, G., and Coauthors, 2015: CORDEX scenarios for Europe from the Rossby Centre regional climate model RCA4. SMHI Rep. Meteorology and Climatology 116, 84 pp., https://www.smhi.se/polopoly_fs/1.90273!/Menu/general/extGroup/attachmentColHold/mainCol1/file/RMK_116.pdf.

Tabari, H., 2010: Evaluation of reference crop evapotranspiration equations in various climates. *Water Resour. Manage.*, **24**, 2311–2337, https://doi.org/10.1007/s11269-009-9553-8.

——, and P. Willems, 2018: More prolonged droughts by the end of the century in the Middle East. *Environ. Res. Lett.*, **13**, 104005, https://doi.org/10.1088/1748-9326/aae09c.

Tangang, F., and Coauthors, 2018: Future changes in annual precipitation extremes over Southeast Asia under global warming of 2°C. *APN. Sci. Bull.*, **8**, 3–8, https://doi.org/10.30852/SB.2018.436.

Taylor, K. E., R. J. Stouffer, and G. A. Meehl, 2012: An overview of CMIP5 and the experiment design. *Bull. Amer. Meteor. Soc.*, **93**, 485–498, https://doi.org/10.1175/BAMS-D-11-00094.1.

Teichmann, C., and Coauthors, 2013: How does a regional climate model modify the projected climate change signal of the driving GCM: A study over different CORDEX regions using REMO. *Atmosphere*, **4**, 214–236, https://doi.org/10.3390/atmos4020214.

Temesgen, B., R. G. Allen, and D. T. Jensen, 1999: Adjusting temperature parameters to reflect well-watered conditions.

J. Irrig. Drain. Eng., **125**, 26–33, https://doi.org/10.1061/(ASCE)0733-9437(1999)125:1(26).

Thomas, D. S., O. V. Wilhelmi, T. N. Finnessey, and V. Deheza, 2013: A comprehensive framework for tourism and recreation drought vulnerability reduction. *Environ. Res. Lett.*, **8**, 044004, https://doi.org/10.1088/1748-9326/8/4/044004.

Thornthwaite, C. W., 1948: An approach toward a rational classification of climate. *Geogr. Rev.*, **38**, 55–94, https://doi.org/10.2307/210739.

Torma, C., F. Giorgi, and E. Coppola, 2015: Added value of regional climate modeling over areas characterized by complex terrain-precipitation over the Alps. *J. Geophys. Res. Atmos.*, **120**, 3957–3972, https://doi.org/10.1002/2014JD022781.

Touma, D., M. Ashfaq, M. A. Nayak, S.-C. Kao, and N. S. Diffenbaugh, 2015: A multi-model and multi-index evaluation of drought characteristics in the 21st century. *J. Hydrol.*, **526**, 196–207, https://doi.org/10.1016/j.jhydrol.2014.12.011.

Tramblay, Y., D. Ruelland, S. Somot, R. Bouaicha, and E. Servat, 2013: High-resolution Med-CORDEX regional climate model simulations for hydrological impact studies: A first evaluation of the ALADIN-Climate model in Morocco. *Hydrol. Earth Syst. Sci.*, **17**, 3721–3739, https://doi.org/10.5194/hess-17-3721-2013.

Trenberth, K. E., and J. T. Fasullo, 2012: Climate extremes and climate change: The Russian heat wave and other climate extremes of 2010. *J. Geophys. Res.*, **117**, D17103, https://doi.org/10.1029/2012JD018020.

——, A. Dai, G. van der Schrier, P. D. Jones, J. Barichivich, K. R. Briffa, and J. Sheffield, 2014: Global warming and changes in drought. *Nat. Climate Change*, **4**, 17–22, https://doi.org/10.1038/nclimate2067.

Ukkola, A. M., A. J. Pitman, M. G. De Kauwe, G. Abramowitz, N. Herger, J. P. Evans, and M. Decker, 2018: Evaluating CMIP5 model agreement for multiple drought metrics. *J. Hydrometeor.*, **19**, 969–988, https://doi.org/10.1175/JHM-D-17-0099.1.

Um, M. J., Y. Kim, and J. Kim, 2017: Evaluating historical drought characteristics simulated in CORDEX East Asia against observations. *Int. J. Climatol.*, **37**, 4643–4655, https://doi.org/10.1002/joc.5112.

van Dijk, A. I. J. M., H. E. Beck, R. S. Crosbie, R. A. de Jeu, Y. Y. Liu, G. M. Podger, B. Timbal, and N. R. Viney, 2013: The Millennium Drought in southeast Australia (2001–2009): Natural and human causes and implications for water resources, ecosystems, economy, and society. *Water Resour. Res.*, **49**, 1040–1057, https://doi.org/10.1002/wrcr.20123.

Vangelis, H., M. Spiliotis, and G. Tsakiris, 2011: Drought severity assessment based on bivariate probability analysis. *Water Resour. Manage.*, **25**, 357–371, https://doi.org/10.1007/s11269-010-9704-y.

van Meijgaard, E., L. H. van Ulft, W. J. van de Berg, F. C. Bosveld, B. J. J. M. van den Hurk, G. Lenderink, and A. P. Siebesma, 2008: The KNMI regional atmospheric climate model RACMO version 2.1. KNMI Tech. Rep. 302, 43 pp., http://bibliotheek.knmi.nl/knmipubTR/TR302.pdf.

van Vuuren, D. P., and T. R. Carter, 2014: Climate and socio-economic scenarios for climate change research and assessment: Reconciling the new with the old. *Climatic Change*, **122**, 415–429, https://doi.org/10.1007/s10584-013-0974-2.

——, and Coauthors, 2011: The representative concentration pathways: An overview. *Climatic Change*, **109**, 5–31, https://doi.org/10.1007/s10584-011-0148-z.

Vicente-Serrano, S. M., S. Beguería, and J. I. López-Moreno, 2010: A multiscalar drought index sensitive to global warming: The standardized precipitation evapotranspiration index. *J. Climate*, **23**, 1696–1718, https://doi.org/10.1175/2009JCLI2909.1.

——, and Coauthors, 2011: Effects of warming processes on droughts and water resources in the NW Iberian Peninsula (1930–2006). *Climate Res.*, **48**, 203–212, https://doi.org/10.3354/cr01002.

——, and Coauthors, 2013: Response of vegetation to drought time-scales across global land biomes. *Proc. Natl. Acad. Sci. USA*, **110**, 52–57, https://doi.org/10.1073/pnas.1207068110.

Vogt, J. V., and F. Somma, Eds., 2000: *Drought and Drought Mitigation in Europe*, Vol. 14, Advances in Natural and Technological Hazards Research Series, Springer, 328 pp.

Voldoire, A., and Coauthors, 2013: The CNRM-CM5.1 global climate model: Description and basic evaluation. *Climate Dyn.*, **40**, 2091–2121, https://doi.org/10.1007/s00382-011-1259-y.

Wang, G., 2005: Agricultural drought in a future climate: Results from 15 global climate models participating in the IPCC 4th assessment. *Climate Dyn.*, **25**, 739–753, https://doi.org/10.1007/s00382-005-0057-9.

Wang, L., and W. Chen, 2014: A CMIP5 multimodel projection of future temperature, precipitation, and climatological drought in China. *Int. J. Climatol.*, **34**, 2059–2078, https://doi.org/10.1002/joc.3822.

——, ——, and W. Zhou, 2014: Assessment of future drought in Southwest China based on CMIP5 multimodel projections. *Adv. Atmos. Sci.*, **31**, 1035–1050, https://doi.org/10.1007/s00376-014-3223-3.

Wang, S. Y., L. Hipps, R. R. Gillies, and J. H. Yoon, 2014: Probable causes of the abnormal ridge accompanying the 2013–2014 California drought: ENSO precursor and anthropogenic warming footprint. *Geophys. Res. Lett.*, **41**, 3220–3226, https://doi.org/10.1002/2014GL059748.

Watanabe, M., and Coauthors, 2010: Improved climate simulation by MIROC5: Mean states, variability, and climate sensitivity. *J. Climate*, **23**, 6312–6335, https://doi.org/10.1175/2010JCLI3679.1.

Wegren, S. K., 2011: Food security and Russia's 2010 drought. *Eurasian Geogr. Econ.*, **52**, 140–156, https://doi.org/10.2747/1539-7216.52.1.140.

Weiß, M., and L. Menzel, 2008: A global comparison of four potential evapotranspiration equations and their relevance to stream flow modelling in semi-arid environments. *Adv. Geosci.*, **18**, 15–23, https://doi.org/10.5194/adgeo-18-15-2008.

Wilhite, D. A., 2000: Drought as a natural hazard: Concepts and definitions. D. A. Wilhite, Ed., *Drought: A Global Assessment*, Vol. 1, Routledge, 1–18.

——, and M. H. Glantz, 1985: Understanding the drought phenomenon: The role of definitions. *Water Int.*, **10**, 111–120, https://doi.org/10.1080/02508068508686328.

——, M. D. Svoboda, and M. J. Hayes, 2007: Understanding the complex impacts of drought: A key to enhancing drought mitigation and preparedness. *Water Resour. Manage.*, **21**, 763–774, https://doi.org/10.1007/s11269-006-9076-5.

Wu, H., M. J. Hayes, D. A. Wilhite, and M. D. Svoboda, 2005: The effect of the length of record on the standardized precipitation index calculation. *Int. J. Climatol.*, **25**, 505–520, https://doi.org/10.1002/joc.1142.

Yevjevich, V. M., 1967: An objective approach to definitions and investigations of continental hydrologic droughts. Colorado State University Hydrology Paper 23, 18 pp., https://mountainscholar.org/bitstream/handle/10217/61303/HydrologyPapers_n23.pdf;sequence=1.

Zahradníček, P., A. Farda, P. Skalák, M. Trnka, J. Meitner, and K. Rajdl, 2016: Projection of drought-inducing climate conditions in the Czech Republic according to Euro-CORDEX models. *Climate Res.*, **70**, 179–193, https://doi.org/10.3354/CR01424.

Zhang, W., C. Jansson, P. A. Miller, B. Smith, and P. Samuelsson, 2014: Biogeophysical feedbacks enhance the Arctic terrestrial carbon sink in regional Earth system dynamics. *Biogeosciences*, **11**, 5503–5519, https://doi.org/10.5194/bg-11-5503-2014.

Zhao, T., and A. Dai, 2015: The magnitude and causes of global drought changes in the twenty-first century under a low–moderate emissions scenario. *J. Climate*, **28**, 4490–4512, https://doi.org/10.1175/JCLI-D-14-00363.1.

——, and ——, 2017: Uncertainties in historical changes and future projections of drought. Part II: Model-simulated historical and future drought changes. *Climatic Change*, **144**, 535–548, https://doi.org/10.1007/s10584-016-1742-x.

Zittis, G., 2018: Observed rainfall trends and precipitation uncertainty in the vicinity of the Mediterranean, Middle East and North Africa. *Theor. Appl. Climatol.*, **134**, 1207–1230, https://doi.org/10.1007/s00704-017-2333-0.

——, P. Hadjinicolaou, and J. Lelieveld, 2014: Comparison of WRF model physics parameterizations over the MENA-CORDEX domain. *Amer. J. Climate Change*, **3**, 490–511, https://doi.org/10.4236/ajcc.2014.35042.